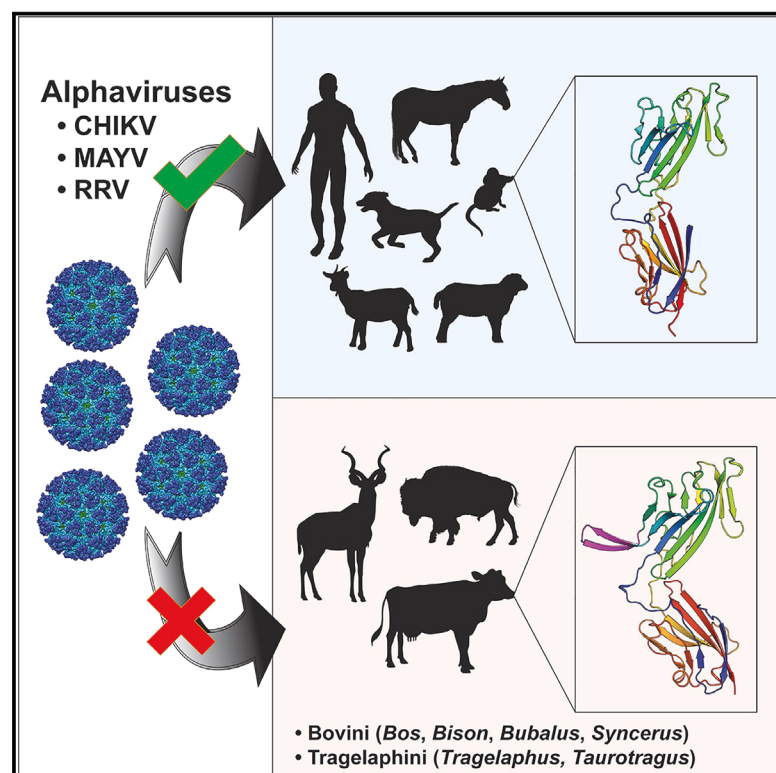# Cell Host & Microbe

An Evolutionary Insertion in the Mxra8 Receptor-Binding Site Confers Resistance to Alphavirus Infection and Pathogenesis

Graphical Abstract

Authors

Arthur S. Kim, Ofer Zimmerman, Julie M. Fox, ..., Michael J. Landis, Daved H. Fremont, Michael S. Diamond

Correspondence

michael.landis@wustl.edu (M.J.L.), fremont@wustl.edu (D.H.F.), diamond@wusm.wustl.edu (M.S.D.)

In Brief

Kim et al. identify a sequence insertion in the Mxra8 receptor of Bovinae species that prevents alphavirus binding. Deletion of the Bovinae Mxra8 insertion restores alphavirus infection, while mice engineered with the Mxra8 insertion exhibit reduced CHIKV infection. Identification of this insertion could facilitate countermeasures preventing Mxra8 engagement of alphaviruses.

Highlights

- An insertion in Bovinae Mxra8 sterically blocks alphavirus binding and infection

- The sequence insertion evolved in the Miocene epoch at least 5 million years ago

- Loss of the insertion in Mxra8 in several Bovinae restores alphavirus infection

- Introduction of the insertion into Mxra8 of mice prevents alphavirus pathogenesis

CellPress

An Evolutionary Insertion in the Mxra8 Receptor-Binding Site Confers Resistance to Alphavirus Infection and Pathogenesis

Arthur S. Kim,[1,2,16] Ofer Zimmerman,[1,16] Julie M. Fox,[1] Christopher A. Nelson,[2] Katherine Basore,[2] Rong Zhang,[1,15] Lorellin Durnell,[1] Chandni Desai,[2] Christopher Bullock,[2] Sharon L. Deem,[7] Jonas Oppenheimer,[8] Beth Shapiro,[9,10] Ting Wang,[3] Sara Cherry,[11] Carolyn B. Coyne,[12] Scott A. Handley,[2] Michael J. Landis,[13,14,*] Daved H. Fremont,[2,4,5,*] and Michael S. Diamond[1,2,4,6,17,*]

[1]Department of Medicine, Washington University School of Medicine, Saint Louis, MO 63110, USA
[2]Department of Pathology and Immunology, Washington University School of Medicine, Saint Louis, MO 63110, USA
[3]Department of Genetics, Washington University School of Medicine, Saint Louis, MO 63110, USA
[4]Department of Molecular Microbiology, Washington University School of Medicine, Saint Louis, MO 63110, USA
[5]Department of Biochemistry and Molecular Biophysics, Washington University School of Medicine, Saint Louis, MO 63110, USA
[6]Andrew M. and Jane M. Bursky the Center for Human Immunology and Immunotherapy Programs, Washington University School of Medicine, Saint Louis, MO 63110, USA
[7]Saint Louis Zoo Institute for Conservation Medicine, Saint Louis, MO 63110, USA
[8]Department of Biomolecular Engineering, University of California, Santa Cruz, Santa Cruz, CA 95064, USA
[9]Department Ecology and Evolutionary Biology, University of California, Santa Cruz, Santa Cruz, CA 95064, USA
[10]Howard Hughes Medical Institute, University of California, Santa Cruz, Santa Cruz, CA 95064, USA
[11]Department of Microbiology, University of Pennsylvania, Philadelphia, PA 19104, USA
[12]Department of Pediatrics, University of Pittsburgh School of Medicine, Pittsburgh, PA 15219, USA
[13]Department of Biology, Washington University, Saint Louis, MO 63110, USA
[14]Department of Ecology and Evolutionary Biology, Yale University, New Haven, CT 06520, USA
[15]Key Laboratory of Medical Molecular Virology (MOE/NHC/CAMS), School of Basic Medical Sciences, Shanghai Medical College, Fudan University, Shanghai 200032, China
[16]These authors contributed equally
[17]Lead Contact
*Correspondence: michael.landis@wustl.edu (M.J.L.), fremont@wustl.edu (D.H.F.), diamond@wusm.wustl.edu (M.S.D.)
https://doi.org/10.1016/j.chom.2020.01.008

SUMMARY

Alphaviruses are emerging, mosquito-transmitted RNA viruses with poorly understood cellular tropism and species selectivity. Mxra8 is a receptor for multiple alphaviruses including chikungunya virus (CHIKV). We discovered that while expression of mouse, rat, chimpanzee, dog, horse, goat, sheep, and human Mxra8 enables alphavirus infection in cell culture, cattle Mxra8 does not. Cattle *Mxra8* encodes a 15-amino acid insertion in its ectodomain that prevents Mxra8 binding to CHIKV. Identical insertions are present in zebu, yak, and the extinct auroch. As other Bovinae lineages contain related Mxra8 sequences, this insertion likely occurred at least 5 million years ago. Removing the Mxra8 insertion in Bovinae enhances alphavirus binding and infection, while introducing the insertion into mouse Mxra8 blocks CHIKV binding, prevents infection by multiple alphaviruses in cells, and mitigates CHIKV-induced pathogenesis in mice. Our studies on how this insertion provides resistance to CHIKV infection could facilitate countermeasures that disrupt Mxra8 interactions with alphaviruses.

INTRODUCTION

Alphaviruses are emerging, mosquito-transmitted positive-sense RNA viruses that cause explosive disease outbreaks in humans and animals. These viruses are classified into groups based on their genetic relatedness and historical boundaries. Old World alphaviruses, including chikungunya (CHIKV), Mayaro (MAYV), O'nyong'nyong (ONNV), and Ross River (RRV), cause acute and chronic musculoskeletal disease affecting millions of people globally. New World alphaviruses, including Eastern (EEEV), Venezuelan (VEEV), and Western (WEEV) equine encephalitis viruses, infect the central nervous system of humans and some animal species. Despite the epidemic potential of alphaviruses, there are no licensed therapies or vaccines for any family member.

The alphavirus RNA genome encodes four non-structural and five structural proteins using two open reading frames (Strauss et al., 1994). The non-structural proteins are required for virus translation, replication, and immune evasion, and the structural proteins (capsid (C) and envelope (E3-E2-6K-E1)) form the virion. The E1 glycoprotein participates in pH-dependent fusion in the acidified endosome (Lescar et al., 2001), and the E2-E1 glycoproteins bind to cellular factors (Smith et al., 1995; Zhang et al., 2005) and facilitate endocytosis (DeTulleo and Kirchhausen, 1998; Lee et al., 2013). The E3 protein is necessary for the folding of the E2-E1 heterodimer (Carleton et al., 1997; Mulvey and Brown, 1995) but is cleaved during the maturation process

(Heidner et al., 1996). Mature enveloped alphaviruses form at the plasma membrane with 240 E2-E1 heterodimers assembled into 80 trimeric icosahedral spikes (Cheng et al., 1995; Kostyuchenko et al., 2011; Paredes et al., 1993; Voss et al., 2010).

The basis for receptor engagement, cellular tropism, and species selectivity of alphaviruses is poorly understood. Attachment factors including heparan sulfates have been shown to enhance infection of some alphaviruses (Gardner et al., 2011; Klimstra et al., 1998; Wang et al., 1992). Natural resistance-associated macrophage protein (NRAMP2) has been described as a receptor for SINV but not for CHIKV or RRV (Rose et al., 2011). We identified Mxra8 as a cellular receptor for multiple Old World arthritogenic alphaviruses including CHIKV, MAYV, ONNV, and RRV (Zhang et al., 2018a). Expression of Mxra8 facilitated alphavirus binding to and infection of mouse and human fibroblasts, skeletal muscle cells, and chondrocytes and was required for virulence in mice (Zhang et al., 2018a, 2019). Mxra8 binds to alphaviruses by wedging into a cleft formed by adjacent E2-E1 heterodimers in one trimeric spike and engaging a neighboring spike (Basore et al., 2019; Song et al., 2019). Apart from its role as an alphavirus receptor, the physiological function of Mxra8 is uncertain. Mxra8 also has been termed adipocyte specific protein 3 (ASP3), limitrin, and dual immunoglobulin domain-containing adhesion molecule (DICAM) because of reported functions in mesenchymal cell differentiation, blood-brain barrier homeostasis, osteoclast development, and angiogenesis (Han et al., 2013; Jung et al., 2004, 2008, 2012; Yonezawa et al., 2003). Although Mxra8 has these ascribed functions, genetically deficient mice are viable and fertile (Han et al., 2019; Zhang et al., 2019).

Because alphaviruses in nature infect humans and several other animal hosts, here, we tested the ability of mammalian Mxra8 orthologs to facilitate infection. Whereas many mammalian Mxra8 genes support CHIKV infection in complementation studies in Mxra8-deficient cells, surprisingly cattle Mxra8 does not. Genetic and structural analysis reveal that the ectodomain of cattle Mxra8 contains a 15-amino acid insertion in the C'-C'' loop of domain 1 (D1), which sterically blocks alphavirus binding and infection. Deletion of this insertion restores the ability of cattle Mxra8 to bind CHIKV and promotes infection by multiple alphaviruses. Reciprocally, introduction of the insert into the corresponding site of mouse Mxra8 abrogates CHIKV binding and infection. Indeed, CRISPR-Cas9-engineered mice containing mouse Mxra8 with the 15-amino acid cattle insertion phenocopy Mxra8 knockout (KO) mice (Zhang et al., 2019) with markedly diminished CHIKV infection and disease, confirming a loss-of-function allele in vivo. Detailed evolutionary analysis reveals that the insertion was present at the same site in most Bovinae family members, which dates its origin to the Miocene epoch. Overall, our experiments explain how an evolutionarily ancient sequence insertion impacts alphavirus-Mxra8 receptor interactions and species tropism and provides a path for developing countermeasures to limit these globally concerning and emerging pathogens.

RESULTS AND DISCUSSION

Alphavirus Infection of Mxra8 Orthologs
Gene editing of Mxra8 results in markedly diminished alphavirus infection and viral infectivity is restored following complementa-

tion with mouse Mxra8 or human MXRA8 (Zhang et al., 2018a). Because many alphaviruses infect other vertebrate hosts in epizootic cycles (Weaver et al., 2012), we tested whether Mxra8 orthologs (Figure 1A) support infection of arthritogenic alphaviruses. We complemented 3T3 fibroblasts lacking Mxra8 expression (ΔMxra8) with Mxra8 from mouse (Mus musculus, positive control), rat (Rattus norvegicus), chimpanzee (Pan troglodytes), dog (Canis lupus familiaris), horse (Equus caballus), cattle (Bos taurus), goat (Capra hircus), and sheep (Ovis aries), which vary by 7%–25% at the nucleotide level and 6%–24% at the amino acid level (Table S1). We also tested whether Mxra8 of three avian species, turkey (Meleagris gallopavo), duck (Anas platyrhynchos), and chicken (Gallus gallus), which vary by ~45% at the amino acid level from mouse Mxra8, promote CHIKV infection. Although birds are not a common amplifying host for arthritogenic alphaviruses (Suhrbier et al., 2012), they act as a reservoir for some encephalitic alphaviruses (Weaver et al., 1999). Surface expression of the different Mxra8 orthologs was confirmed with cross-reactive monoclonal antibodies (mAbs) against Mxra8 (Zhang et al., 2018a) or antibodies against an N-terminal tag placed downstream of the signal peptide (Figures S1A, S1B, S1E, and S1F). Complemented cells were inoculated with CHIKV (strain 181/25) and evaluated for infection by quantifying intracellular viral E2 protein expression by flow cytometry. Consistent with previous findings (Zhang et al., 2018a), the CHIKV E2 antigen was absent in ΔMxra8 cells but present at high levels in ΔMxra8 cells complemented with mouse Mxra8. Complementation of ΔMxra8 cells with rat, chimpanzee, dog, horse, goat, and sheep Mxra8 orthologs also restored CHIKV infectivity (Figures 1B and 1C). However, Mxra8 from cattle and the three more distantly related avian species failed to restore infectivity despite comparable surface expression (Figures 1B, 1C, S1C, and S1D). Of note, the N-terminal tag used to detect the avian constructs did not diminish the ability of mouse Mxra8 to support CHIKV infection (Figure S1C). Similar results were observed with other CHIKV strains (AF15561 and LR-2006) and MAYV and RRV (Figures 1D–1H). In contrast, expression of the mammalian Mxra8 orthologs did not enhance infection of VEEV, an encephalitic alphavirus (Figure 1I). These data are consistent with previous results showing that mouse Mxra8 expression exclusively enhances infection of arthritogenic alphaviruses (Zhang et al., 2018a).

Cattle Mxra8 Contains a Repeat Sequence Insertion
To define the mechanism by which cattle Mxra8 fails to promote alphavirus infectivity, we first aligned its sequence with mouse Mxra8. Cattle Mxra8 contains a 15-amino acid insertion composed of three quasi-identical (GEQRL/V) five-residue repeats that appear to be derived from an immediately adjacent GEQRV gene sequence (Figure S2A). These sequences are encoded by GC-rich tandem repeats and expand a CpG island (Figure S2B) while preserving the protein coding frame. CpG islands often are hypomethylated (Roadmap Epigenomics Consortium et al., 2015) and associated with genome instability (Du et al., 2014). Thus, analogous to well-characterized structural variations in human coding exons (Challis et al., 2015; Montgomery et al., 2013), this GC-rich region is prone to form a single-stranded DNA loop (Figure S2C) as a consequence of
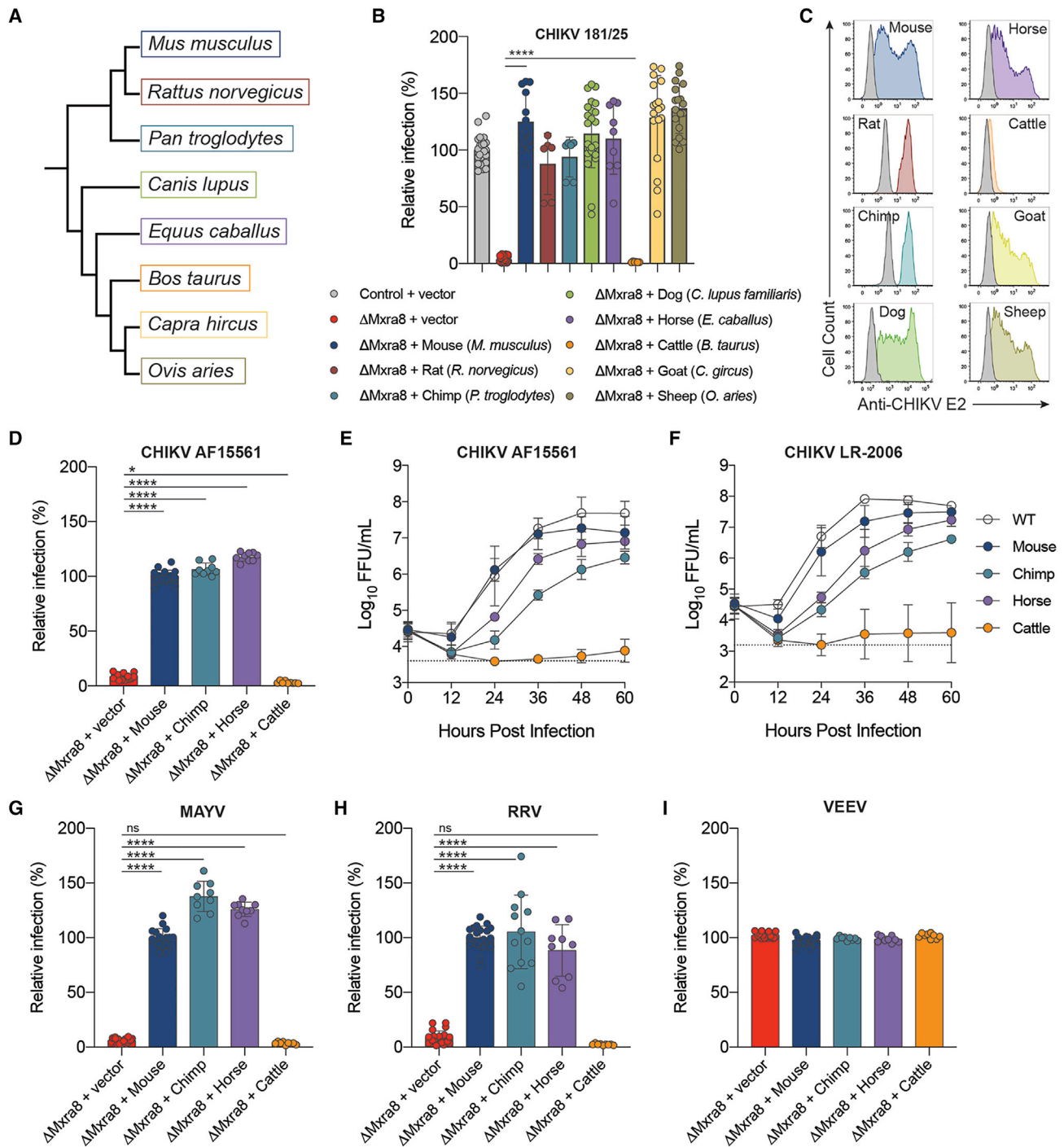
Figure 1. Alphavirus Infection of Cells Expressing Mxra8 Gene Orthologs

(A) Dendrogram of mammalian Mxra8 genes.

(B and C) Lentivirus complementation of Δ*Mxra8* 3T3 with Mxra8 cDNA from mouse, rat, chimpanzee, dog, horse, cattle, goat, and sheep. Cells were inoculated with CHIKV (181/25) and analyzed for infection by staining with anti-E2 mAbs. Infection data are the mean ± SD pooled from three to nine experiments (n = 6 to 24 replicates; one-way ANOVA with Dunnett's post-test: ****$p < 0.0001$) (B) and representative flow cytometry plots of infected cells (C) are shown. Small differences in infection of some species (e.g., chimp and horse) may reflect relative levels of expression of the Mxra8 orthologs (see Figure S1) or inherent differences in affinity of binding.

(D–I) Lentivirus complementation of Δ*Mxra8* 3T3 with Mxra8 cDNA from mouse, cattle, horse, and chimpanzee. Cells were inoculated with (D) and (E) CHIKV (AF15561), (F) CHIKV (LR-2006) (G) MAYV (BeH407), (H) RRV (T48), or (I) VEEV (TC-83) and stained with virus-specific anti-E2 mAbs to quantify the infection (see STAR Methods). For (E) and (F), a multi-step growth analysis was conducted and virus was titrated by the focus-forming assay. Data are the mean ± SD pooled from three experiments performed in triplicate (one-way ANOVA with Dunnett's post-test: *$p < 0.05$; ****$p < 0.0001$; n.s., not significant).
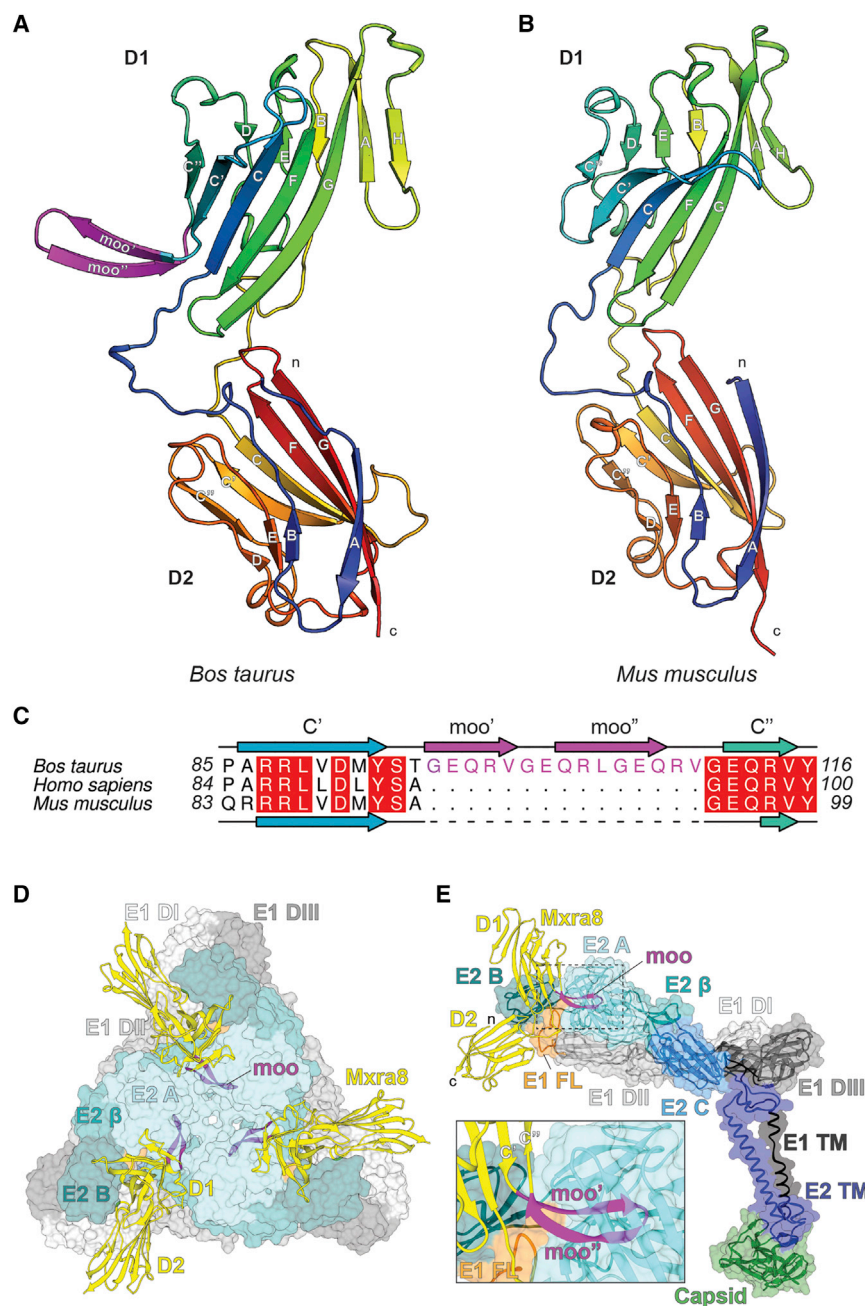
See Figure S1.

Figure 2. Structure of Cattle Mxra8

(A and B) Ribbon models of the (A) cattle and (B) mouse Mxra8 (PDB 6NK3) structures determined by X-ray crystallography. The two Ig-like domains are colored by Jones' rainbow scheme with the N terminus in blue and C terminus in red. The β-strands of each Ig domain are labeled according to standard convention. The N and C termini are labeled in lowercase.

(C) Structure-based alignment of *Bos taurus* (cattle), *Homo sapiens* (human), and *Mus musculus* (mouse) Mxra8 protein sequences highlighting the 15-amino acid insertion site between the C' and C'' loop in D1.

(D and E) Docking of cattle Mxra8 onto a cryo-EM model of mouse Mxra8 bound to CHIKV VLPs, viewed from a trimeric spike (D), an E2-E1 subunit (E), and enlarged to highlight the clash (inset). Cattle Mxra8 is colored yellow and labeled by domain, with the moo insert depicted in magenta. The N and C termini are labeled in lowercase. Within the inset, the C', "moo" insert, and C'' β-strands are labeled and the E1 fusion loop is depicted in orange. Structural proteins are colored and labeled by domain. E1: DI, light gray; DII, medium gray; DIII, dark gray; fusion loop, orange; and TM region, black. E2: A domain, light cyan; β-linker, medium cyan; domain B, dark cyan; domain C, medium blue; and TM region, dark blue. Capsid, green.

See Figures S2 and S3.

(Basore et al., 2019). This domain rotation is similar to that in unliganded murine Mxra8 (Basore et al., 2019) and unlikely to explain why cattle Mxra8 does not support alphavirus infection. Weak electron density for the 15-amino acid insertion of cattle Mxra8 indicates it can form a β-hairpin loop (herein termed moo' and moo'' strands), which projects away from D1 between the C' and C'' loops (Figures 2A, 2C, and S3C). This inserted region appears to be stabilized by crystal lattice contacts with an adjacent symmetry mate, suggesting that this might not be the only conformation of the "moo" loop.

We docked cattle Mxra8 coordinates onto the cryo-electron microscopy structure of CHIKV virions in complex with mouse Mxra8 (Basore et al., 2019) (Figures 2D and 2E). These analyses suggest that the modeled 15-amino acid insertion sterically hinders Mxra8 binding to the CHIKV virion, as the insertion physically clashes with residues in domain A of the CHIKV E2 protein on the heterotrimeric spike. Superimposition of cattle Mxra8 into the crystal structure of CHIKV E3-E2-E1 proteins bound to human MXRA8 (Song et al., 2019) also indicates clashes between the insertion and domain A of the CHIKV E2 protein. These docking studies suggest that cattle Mxra8 could not productively engage the CHIKV virion even if a different conformation of the 15-amino acid insertion were adopted, as alternate steric clashes would be generated. In

polymerase slippage during DNA replication (Tian et al., 2011), which may have caused the nucleotide insertion in *Mxra8*.

Structural Analysis of Cattle Mxra8

We expressed cattle Mxra8 protein in *E. coli* (Figures S3A and S3B) and obtained a 2.3 Å crystal structure (Figure 2A; Table S2). Cattle Mxra8, similar to mouse Mxra8, adopts two immunoglobulin (Ig)-like domains (Figures 2A and 2B) that position in an unusual head-to-head orientation with a disulfide bond linkage between them (Figure S3C) (Basore et al., 2019; Song et al., 2019). The two domains of cattle Mxra8 are connected by a hinge, with ~31° of movement in the position of domain D1 relative to D2 compared with mouse Mxra8 when bound to CHIKV
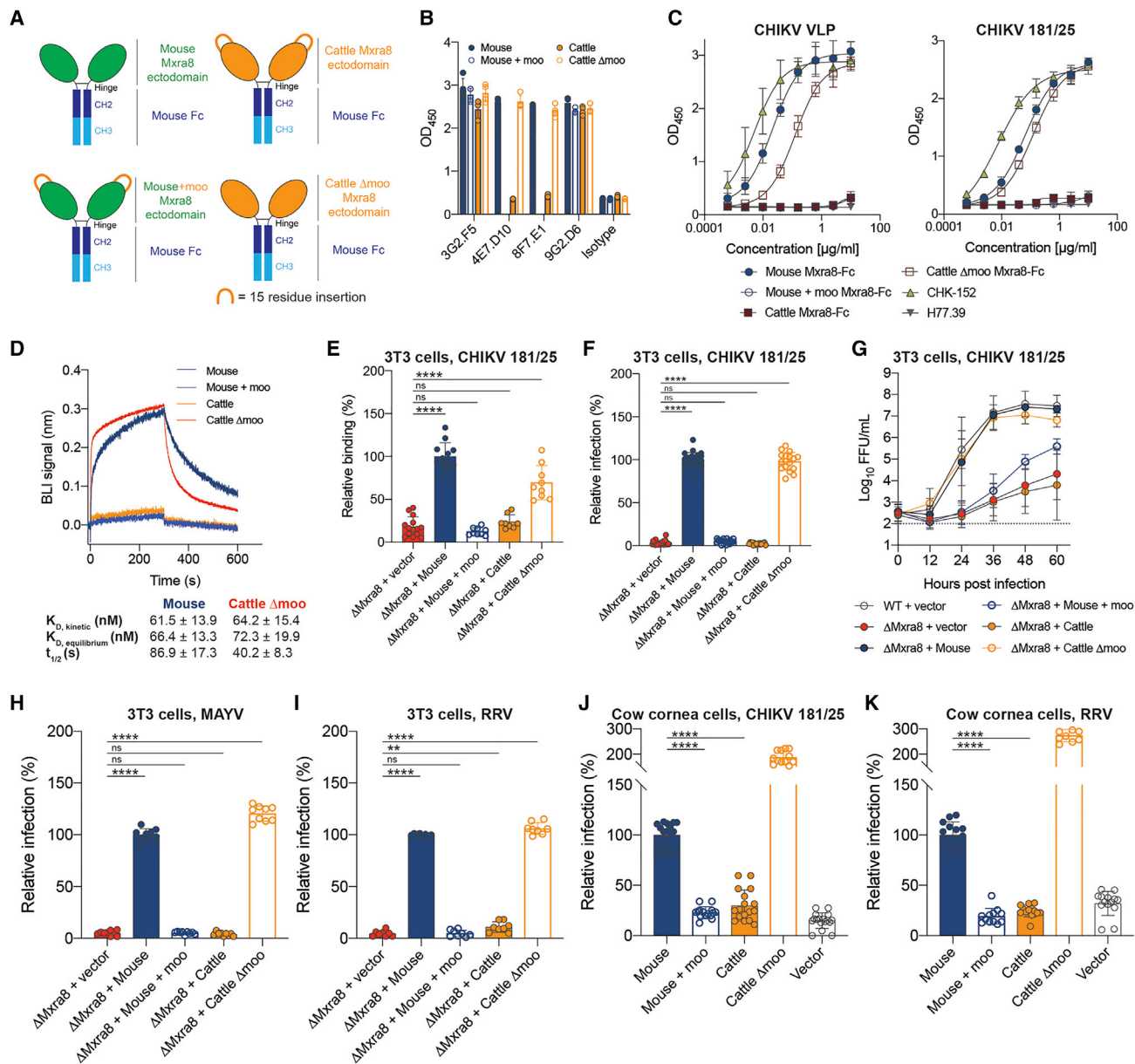
Figure 3. Effect of the 15-Amino Acid Insertion in Cattle Mxra8 on Alphavirus Binding and Infection

(A) Diagram of mouse, cattle, mouse + moo [GEQRVGEQRLGEQRV insert], and cattle Δmoo Mxra8-Fc fusion proteins.

(B) Binding of anti-Mxra8 mAbs 3G2.F5, 4E7.D10, 8F7.E1, and 9G2.D6 to mouse, cattle, mouse + moo, and cattle Δmoo Mxra8-Fc fusion proteins by ELISA. Data are the mean ± SD pooled from four experiments performed in duplicate.

(C) Binding of increasing concentrations of mouse, cattle, mouse + moo, and cattle Δmoo Mxra8-Fc fusion proteins to antibody-captured CHIKV VLPs and CHIKV 181/25 virions by ELISA. Data are the mean ± SD pooled from two to three experiments performed in duplicate.

(D) Representative kinetic sensograms of bacterially expressed mouse (blue), mouse + moo (light blue), cattle (orange), and cattle Δmoo (red) Mxra8 binding to CHIKV VLPs as determined by BLI. CHIKV VLPs were captured using an anti-CHIKV mAb (CHK-265) and then incubated with Mxra8 proteins. Binding data represent the mean of three experiments.

(E) Binding of CHIKV 181/25 virions to 3T3 Δ*Mxra8* cells complemented with mouse, mouse + moo, cattle, or cattle Δmoo Mxra8 cDNA. Virions were incubated with cells at 4°C and CHIKV antigen staining was analyzed by flow cytometry. Data are the mean ± SD pooled from three to four experiments (n = 9 to 14 replicates; one-way ANOVA with Dunnett's post-test: ****p < 0.0001).

(F–I) Lentivirus complementation of 3T3 Δ*Mxra8* cells with Mxra8 cDNA from mouse, mouse + moo, cattle, and cattle Δmoo. Cells were inoculated with (F) and (G) CHIKV (181/25), (H) MAYV (BeH407), or (I) RRV (T48). For (G), a multi-step growth analysis was conducted, and virus was titrated by the focus-forming unit assay. Data are the mean ± SD pooled from three experiments performed in sextuplicate. For (F), (H), and (I), cells were processed at specified time points (see STAR Methods) and stained with virus-specific anti-E2 protein mAbs.

(legend continued on next page)

comparison, structure-function analysis of avian Mxra8 orthologs, which also do not promote CHIKV infection, showed no insertions, but instead revealed sequence variation at the virus-receptor interface (Basore et al., 2019; Song et al., 2019) with substitutions in 17 different contact residues (Figure S1G) relative to mouse Mxra8.

The Insertion in Cattle Mxra8 Restricts Alphavirus Binding and Infection

To determine whether the insertion in cattle Mxra8 disrupts interactions with CHIKV virions, we engineered mouse and cattle Mxra8-Fc fusion proteins with or without the additional 15 residues from cattle (hereafter termed the "moo" insert: mouse Mxra8-Fc, mouse Mxra8 + moo-Fc, cattle Mxra8-Fc, and cattle Mxra8 Δmoo-Fc) (Figures 3A and S3D). We evaluated antigenic integrity of the chimeric proteins by assessing binding to four cross-reactive anti-Mxra8 mAbs (Zhang et al., 2018a) that engage multiple epitopes (Basore et al., 2019). MAbs 3G2.F5 and 9G2.D6 bound to all cattle and mouse Mxra8-Fc variants (Figures 3B and S3E), whereas mAbs 4E7.D10 and 8F7.E1 failed to bind efficiently to cattle Mxra8-Fc but recognized mouse Mxra8-Fc and cattle Mxra8 Δmoo-Fc, suggesting they bind an epitope proximal to the 15-amino acid insertion. Consistent with this idea, 4E7.D10 and 8F7.E1 were mapped by hydrogen-deuterium exchange mass spectrometry to residues 91–107 on Mxra8 (Basore et al., 2019).

We tested the Mxra8-Fc fusion proteins for their capacity to bind CHIKV virus-like particles (VLPs) and virions by ELISA. Mouse Mxra8-Fc and cattle Mxra8 Δmoo-Fc bound avidly to CHIKV VLPs and virions, whereas mouse Mxra8 + moo-Fc and cattle Mxra8-Fc did not (Figure 3C). In a complementary approach, we assessed the monovalent binding of purified wild-type (WT) and chimeric Mxra8 proteins to recombinant CHIKV VLPs using bio-layer interferometry (BLI). Mouse Mxra8 ($K_D = 66.4 \pm 13.3$ nM) and cattle Mxra8 Δmoo ($K_D = 72.3 \pm 19.9$ nM) but not mouse Mxra8 + moo and cattle Mxra8 bound to CHIKV VLPs (Figures 3D and S3F; Table S3). Consistent with these results, CHIKV virions bound poorly to 3T3 ΔMxra8 cells expressing mouse Mxra8 + moo or cattle Mxra8 compared to mouse or cattle Δmoo Mxra8 (Figure 3E). These data suggest that the 15-amino acid insertion in cattle Mxra8 inhibits binding to CHIKV and support the structure-based hypothesis that cattle Mxra8 cannot engage the CHIKV spike because of the presence of a protruding loop that sterically blocks binding (Figures 2D and 2E).

To test whether the insertion blocks alphavirus infection, we transduced ΔMxra8 3T3 cells with mouse Mxra8, mouse Mxra8 + moo, cattle Mxra8, or cattle Mxra8 Δmoo. All WT and chimeric Mxra8 variants were detected on the cell surface (Figures S4A and S4B). The addition of the 15-amino acid insertion to mouse Mxra8 abolished infectivity by CHIKV, MAYV, and RRV, whereas its deletion from cattle Mxra8 restored infection to levels observed following transduction of mouse Mxra8 (Figures 3F–3I). To confirm these results in a more species-relevant cell type, we transduced bovine cornea cells with mouse Mxra8, mouse Mxra8 + moo, cattle Mxra8, or cattle Mxra8 Δmoo, followed by inoculation of CHIKV or RRV. These cells lack endogenous surface expression of Mxra8 and at baseline did not support infection of either CHIKV or RRV (Figures S4C–S4E). Bovine cornea cells transduced with mouse Mxra8 or cattle Mxra8 Δmoo but not mouse Mxra8 + moo or cattle Mxra8 were susceptible to CHIKV and RRV infection (Figures 3J–3K, S4D, and S4E).

The 15-Amino Acid Insertion Attenuates CHIKV Infection and Pathogenesis *In Vivo* in CRISPR-Cas9-Engineered Mice

We engineered C57BL/6J knockin (KI) mice with a Mxra8 allele containing the "moo" insertion ($Mxra8^{moo}$) to test its function in alphavirus virulence *in vivo* (Figure 4A). Founder $Mxra8^{moo/moo}$ or WT mice were bred to Mxra8-deficient ($Mxra8^{KO/KO}$) mice (Zhang et al., 2019) or each other to establish Mxra8 "moo" KI ($Mxra8^{moo/KO}$ and $Mxra8^{moo/moo}$) mice and corresponding control animals. All mice containing the Mxra8 "moo" allele developed normally. To confirm expression of Mxra8^{moo} in the KI mice, we probed primary mouse embryonic fibroblasts (MEFs) by performing immunoblotting of lysates and flow cytometry of cells. Whereas $Mxra8^{WT/WT}$ and $Mxra8^{WT/KO}$ MEFs had Mxra8 bands at ∼50 kDa, no band migrating at this mobility was detected in lysates from $Mxra8^{KO/KO}$ MEFs. Immunoblots of $Mxra8^{moo/KO}$ MEFs, however, displayed a band of ∼52 kDa, consistent with the 15-amino-acid "moo" insertion (Figure 4B). We detected cell surface expression of Mxra8 on $Mxra8^{WT/WT}$, $Mxra8^{WT/KO}$, and $Mxra8^{moo/KO}$ MEFs but not $Mxra8^{KO/KO}$ MEFs (Figure 4C). In multi-step growth analysis, both $Mxra8^{WT/WT}$ and $Mxra8^{WT/KO}$ MEFs supported robust CHIKV infection whereas $Mxra8^{KO/KO}$ and $Mxra8^{moo/KO}$ MEFs did not (Figure 4D). We then examined disease by inoculating mice with virulent CHIKV (strain AF15561). Markedly reduced ankle joint swelling was observed throughout the acute phase (days 2 to 10) in $Mxra8^{moo/KO}$ and $Mxra8^{KO/KO}$ compared to $Mxra8^{WT/KO}$ and $Mxra8^{WT/WT}$ mice (Figure 4E). Moreover, at day 3 post-inoculation, the $Mxra8^{moo/KO}$ and $Mxra8^{KO/KO}$ mice displayed diminished viral loads in the serum, ipsilateral and contralateral calf muscles, and contralateral ankles relative to $Mxra8^{WT/WT}$ and $Mxra8^{WT/KO}$ mice (Figures 4G–4J). Similar results were observed after CHIKV infection of homozygous $Mxra8^{moo/moo}$ mice with reduced ankle swelling and viral burden compared to $Mxra8^{WT/WT}$ mice (Figures 4F and 4K–4N). However, low levels of CHIKV were detected in $Mxra8^{moo/KO}$, $Mxra8^{moo/moo}$, and $Mxra8^{KO/KO}$ mice. These results agree with previous cell culture and *in vivo* experiments (Zhang et al., 2018a, 2019) and suggest that a Mxra8-independent entry pathway exists for CHIKV, at least in mice, although it is not sufficient to promote clinical disease. Nonetheless, as CHIKV virulence is diminished in $Mxra8^{moo/KO}$, $Mxra8^{moo/moo}$, and $Mxra8^{KO/KO}$ mice relative to

(J and K) Lentivirus complementation of bovine cornea cells with Mxra8 cDNA of mouse, cattle, mouse + moo, and cattle Δmoo. Cells were inoculated with (J) CHIKV (181/25) or (K) RRV (T48) and processed by staining with anti-E2 protein mAbs. The relative increase in CHIKV and RRV infection in bovine cornea cells expressing cattle Δmoo Mxra8 may reflect the higher levels of surface expression (see Figure S5C).

For (F) and (H)–(K), data are the mean ± SD pooled from three to nine experiments (n = 6 to 26 replicates; one-way ANOVA with Dunnett's post-test: **p < 0.01; ****p < 0.0001).
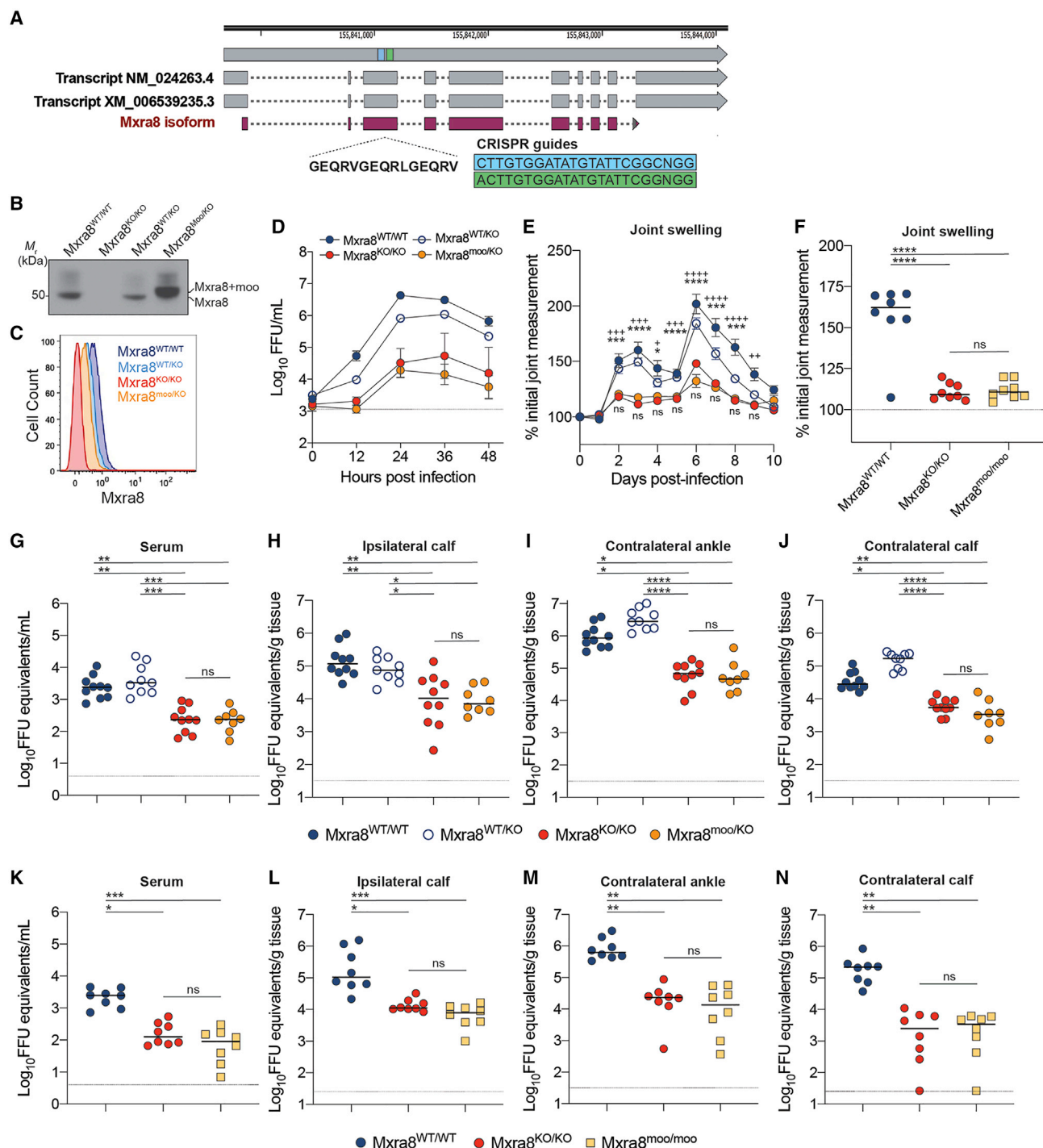
See Figures S3 and S4.

Figure 4. *In Vivo* **Assessment of the Mxra8 "Moo" Insertion**

(A) Generation of Mxra8-moo knockin C57BL/6J mice using CRISPR-Cas9 gene editing. The "moo" insertion (GEQRVGEQRLGEQRV) was introduced into exon 3 of the *Mxra8* gene using two single guide RNAs (sgRNAs) as indicated by the blue and green boxes. Annotated transcripts are shown in gray and the encoded protein in purple.

(B) Immunoblotting of cell lysates from primary Mxra8[WT/WT], Mxra8[KO/KO], Mxra8[WT/KO], and Mxra8[moo/KO] MEFs using anti-Mxra8 mAbs 3G2.F5 and 9G2.D6 (Mr, migration rate). Data are representative of three experiments.

(C) Surface expression of Mxra8 from primary MEFs (Mxra8[WT/WT] (dark blue), Mxra8[KO/KO] (red), Mxra8[WT/KO] (light blue), and Mxra8[moo/KO] (orange)) after staining with a pool of anti-Mxra8 mAbs as determined by flow cytometry. Data are representative of two experiments.
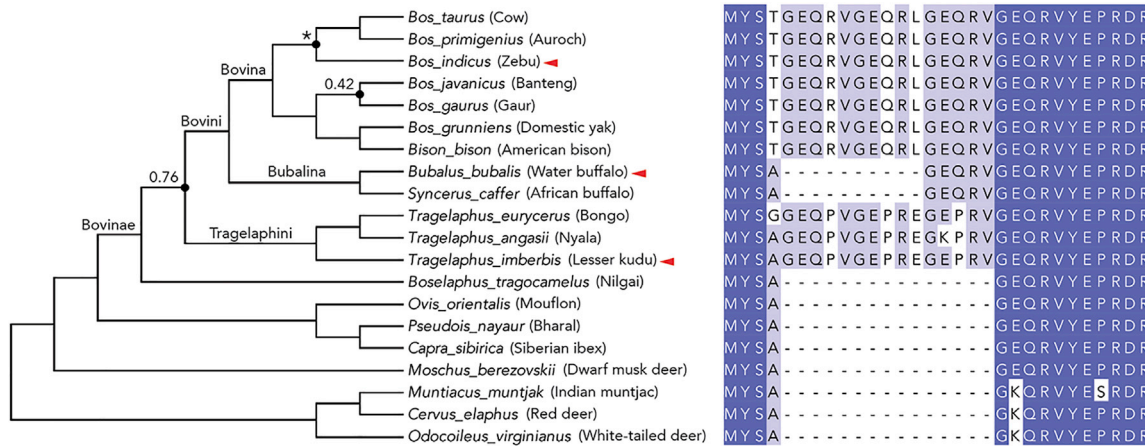
(legend continued on next page)

Figure 5. Phylogenetic Relationship of Mxra8 Orthologs

The phylogeny summarizes the relationships for Bovinae, Bovidae, Moschidae, and Cervidae as estimated by (Zurano et al., 2019) but was modified to include the relationships for *Bos taurus* and *Bos indicus* (reported by Wang et al., 2018) as indicated by asterisks. All nodes have high support with posterior probabilities >95% unless indicated otherwise by values. Species indicated with red arrows are investigated in subsequent functional experiments. The phylogenetic tree and sequence alignment were prepared using FigTree and Jalview (Waterhouse et al., 2009), respectively. Protein sequences of *Mxra8* gene orthologs from Bovidae members in the region corresponding to the 15-residue Mxra8 insertion in D1 were aligned using MUSCLE and visualized using Jalview. Amino acid residues are colored according to sequence identity among Bovidae family members: dark blue boxes (100%), light blue boxes (50%–90%), and white boxes (<50%). Gaps in the protein sequences are indicated by a dash.

$Mxra8^{WT/WT}$ and $Mxra8^{WT/KO}$ mice, the "moo" insertion produces a loss-of-function allele for CHIKV infection *in vivo*.

Mxra8 Insertions Are Present in Most Bovinae Species and Inhibit Alphavirus Infection

We determined whether the 15-amino acid insertion was present in species related to cattle. We evaluated calibrated phylogenetic trees that were developed using autosomal and mitochondrial DNA sequences (MacEachern et al., 2009; Zurano et al., 2019) to identify Bovinae subfamily and Bovidae family members with shared ancestry (Figure 5, left panel). This tree included tribes within the Bovinae subfamily (Bovini, Tragelaphini, and Boselaphini), closely related Bovidae (*Ovis*, *Pseudois*, and *Capra*), and more distantly related Cervidae (*Cervus*, *Muntiacus*, and *Odocoileus*) and Moschidae (*Moschus*) species. We obtained sequences of *Mxra8* gene orthologs (Tables S4 and S5; STAR Methods) by (1) downloading annotated Mxra8 gene sequences from GenBank; (2) assembling deposited; unannotated whole genome or exome sequences; and (3) isolating mRNA from tissues obtained at necropsy from animals at the Saint Louis Zoo, samples acquired from commercial vendors, and validated primary fibroblasts of different Bovinae species (Modi et al., 2004).

All Bovinae subfamily members except one had insertions in *Mxra8* at the same site as observed in cattle. The most distantly related Bovinae member (*Boselaphus tragocamelus*) lacked the insertion as did representatives of Cervidae, Moschidae, and three non-Bovinae members of Bovidae (*Ovis orientalis*, *Pseudois nayaur*, and *Capra sibirica*) (Figure 5, right panel and Figure S5A). Members of the Bovina subtribe (*Bos* and *Bison*) share identical 15-amino acid insertions whereas the Bubalina subtribe (*Bubalus* and *Syncerus*) had 5-amino acid insertions (one GEQRV repeat) at the same site as in cattle. The common ancestor of *Bubalus bubalis* and *Syncerus caffer* may have lost 30 nucleotides of the ancestral insertion. Alternatively, an independent introduction of the GEQRV insertion could have occurred in the ancestor of *Bubalus* and *Syncerus* at the same site in *Mxra8*. Members of the more distantly related Tragelaphus subtribe of spiral-horned antelopes (e.g., nyala (*Tragelaphus angasii*), bongo (*Tragelaphus eurycerus*), and lesser kudu (*Tragelaphus imberbis*)) all had similar 45-nucleotide (89% identity) and 15-amino acid (73% identity) insertions (GEQPVGEPREGEPRV; with three notable proline substitutions) within the same insertion site in *Mxra8*.

To determine the significance of the insertions of other Bovinae species in *Mxra8*, we engineered a panel of Mxra8-Fc fusion proteins including water buffalo (Bubalus)-Fc, water

(D) Multi-step growth analysis of CHIKV AF15561 in primary MEFs ($Mxra8^{WT/WT}$, $Mxra8^{KO/KO}$, $Mxra8^{WT/KO}$, and $Mxra8^{moo/KO}$). Cells were infected at an MOI of 0.01, and virus in supernatants was harvested at the time points shown and titrated by the focus-forming assay. Data are representative of three experiments performed in sextuplicate.

(E–N) $Mxra8^{WT/WT}$, $Mxra8^{KO/KO}$, $Mxra8^{WT/KO}$, $Mxra8^{moo/KO}$, and $Mxra8^{moo/moo}$ mice were inoculated in the footpad with 10^3 focus-forming units (FFU) of CHIKV AF15561. Joint swelling was monitored over 10 days (E) or at day 3 post-infection (F). Viral RNA levels in serum (G) and (K), ipsilateral calf muscle (H) and (L), contralateral ankle (I) and (M), and contralateral calf muscle (J) and (N) were measured at 3 days post-infection. For (E), data are the mean ± SEM from three experiments (n = 11 to 15; two-way ANOVA with Dunnett's post-test: × or +, $p < 0.05$; ** or ++, $p < 0.01$; *** or +++, $p < 0.001$; **** or ++++, $p < 0.0001$; ns, not significant). "*" indicates a comparison between $Mxra8^{WT/WT}$ and $Mxra8^{moo/KO}$. "+" indicates a comparison between $Mxra8^{WT/KO}$ and $Mxra8^{moo/KO}$. "ns" data are a comparison between $Mxra8^{KO/KO}$ and $Mxra8^{moo/KO}$. For (F)–(N), data are from two experiments (n = 8 to 10; one-way ANOVA with Kruskal-Wallis post-test: *$p < 0.05$; **$p < 0.01$; ***$p < 0.001$; ****$p < 0.0001$; ns, not significant).
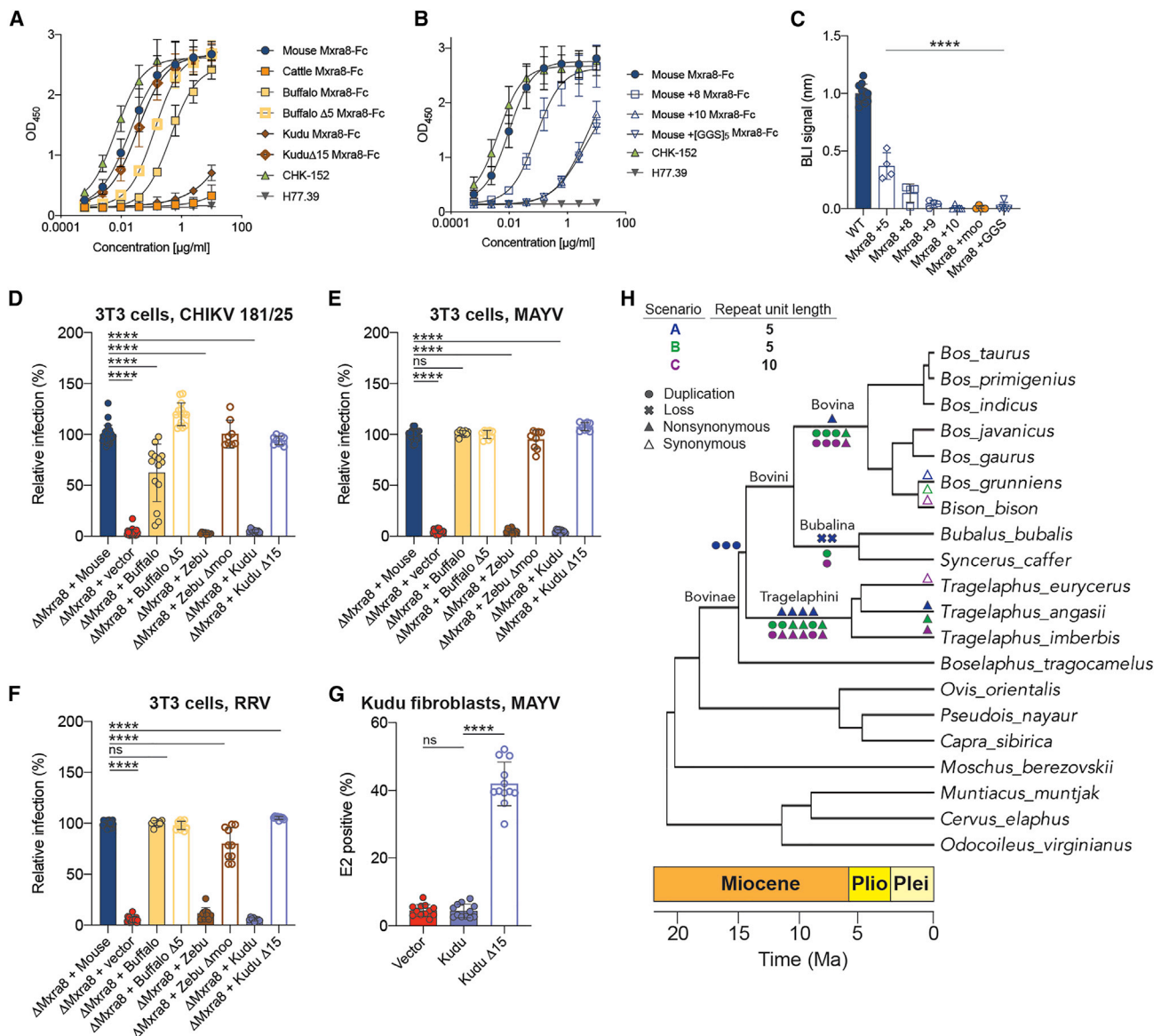
Figure 6. Functional and Evolutionary Relationships of Mxra8

(A) Binding of mouse-Fc, cattle-Fc, water buffalo-Fc, water buffalo-Δ5-Fc, kudu-Fc, and kudu-Δ15-Fc Mxra8 fusion proteins to antibody-captured CHIKV VLPs by ELISA. Data are the mean ± SD pooled from three experiments performed in duplicate.

(B) Binding of mouse-Fc, mouse-Mxra8 + 8-Fc, mouse-Mxra8 + 10-Fc, and mouse-Mxra8 + [GGS]$_5$-Fc fusion proteins to antibody-captured CHIKV by ELISA. MAbs CHK-152 (anti-CHIKV) and H77.39 (anti-HCV) were included as positive and negative controls, respectively. Data are the mean ± SD pooled from three experiments performed in duplicate.

(C) Binding response of the bacterially expressed mouse Mxra8 and insertion variants Mxra8 + 5, Mxra8 + 8, and Mxra8 + 9, Mxra8 + 10, Mxra8 + moo, and Mxra8 + [GGS]$_5$ to antibody-captured CHIKV VLPs at a 1 μM concentration by BLI. Data are the mean ± SD of four to five experiments (one-way ANOVA with Dunnett's post-test: ****p < 0.0001).

(D–F) Lentivirus complementation of Δ*Mxra8* 3T3 with Mxra8 cDNA from water buffalo, water buffalo Δ5, zebu, zebu Δmoo, kudu, and kudu Δ15. Cells were inoculated with (D) CHIKV (181/25), (E) MAYV (BeH407), or (F) RRV (T48); harvested; stained with anti-E2 mAbs; and processed by flow cytometry. For (D)–(F), data are the mean ± SD pooled from three to eight experiments (n = 8 to 23 replicates; one-way ANOVA with Dunnett's post-test: ****p < 0.0001).

(G) MAYV infection of primary kudu fibroblasts transduced with vector control, kudu Mxra8, or kudu Δ15 Mxra8. Data are the mean ± SD from four experiments (n = 12; one-way ANOVA with Dunnett's post-test: ****p < 0.0001; ns, not significant).

(H) Evolutionary scenarios for the Bovinae Mxra8 gene insertions. The three scenarios are based on the length of the repeat unit and whether losses or duplications of the repeat unit are more common. Duplication events are indicated as circles, losses are indicated by "x" marks, nonsynonymous substitutions are indicated as filled triangles, and synonymous substitutions are indicated as open triangles. Events are shown in their reconstructed order, from oldest (left) to youngest (right), and in their youngest possible positions, though the age of any event is not precisely known. All scenarios involve one synonymous substitution occurring within *Bos grunniens* and one nonsynonymous substitution occurring within *Tragelaphus angasii* but differ elsewhere. In scenario A (blue symbols), where the loss of the 5-amino acid repeat unit is relatively common, the repeat unit is duplicated three times in the common ancestor of Bovini and Tragelaphini.

(legend continued on next page)

buffalo-Δ5-Fc, kudu-Fc, and kudu-Δ15-Fc (Figure S5B). We designed three additional variants to define the effect of size and sequence of the insertion on CHIKV binding: mouse-Mxra8 + 8-Fc and mouse-Mxra8 + 10-Fc add 8 (QRVGEQRL) and 10 (GEQRVGEQRL) of the 15 amino acids, respectively, from the cattle, and mouse-Mxra8+[GGS]$_5$-Fc adds 15 non-homologous amino acids (GGSGGSGGSGGSGGS) that are predicted to form a flexible loop (Figure S5C). These Mxra8-Fc fusion proteins were recognized by anti-Mxra8 mAbs (Figure S5D). We tested these Mxra8-Fc proteins for their capacity to bind CHIKV VLPs by ELISA. No binding was detected with kudu-Mxra8-Fc; markedly diminished binding was observed with mouse-Mxra8 + 10-Fc and mouse-Mxra8 + [GGS]$_5$-Fc; intermediate binding was detected with water buffalo Mxra8-Fc and mouse-Mxra8+8-Fc; and avid binding was observed with water buffalo-Δ5-Mxra8-Fc, kudu-Δ15-Mxra8-Fc, and mouse Mxra8-Fc (Figures 6A and 6B). To corroborate these results, we assessed the monovalent binding of purified mouse Mxra8 insertion variants to CHIKV VLPs using BLI. All Mxra8 insertion variants were recognized by an anti-Mxra8 mAb (Figure S5E), suggesting proper folding. Mouse Mxra8 bound strongly to CHIKV VLPs, whereas mouse Mxra8 + 5, mouse Mxra8 + 8, mouse Mxra8 + 9, mouse Mxra8 + 10, mouse Mxra8 + moo, or mouse Mxra8 + [GGS]$_5$ displayed little or no binding (Figure 6C). These data suggest that insertions of as few as five residues at the "moo" site inhibit interactions of Mxra8 with CHIKV, although receptor blockade does not require a specific sequence.

To test whether the 15-residue insertion in other Mxra8 orthologs similarly disrupts alphavirus infection, we complemented ΔMxra8 3T3 cells with water buffalo Mxra8, water buffalo Δ5 Mxra8, zebu Mxra8, zebu Δ15 Mxra8, kudu Mxra8, or kudu Δ15 Mxra8, followed by inoculation with CHIKV, MAYV, or RRV. All WT and sequence-deleted Mxra8 variants were detected on the cell surface (Figure S6A). Whereas zebu and kudu Mxra8 did not promote infection, expression of the respective 15 amino acid deleted forms enabled infection of the viruses tested (Figures 6D–6F and S6B–S6D). Water buffalo Mxra8 had an intermediate phenotype; while it supported MAYV and RRV infection, the level of CHIKV infection was diminished. However, CHIKV infection was increased in cells expressing water buffalo Δ5 Mxra8. In additional experiments, we transduced primary kudu fibroblasts with kudu Mxra8 or kudu Δ15 Mxra8 (Figure S6E). Whereas kudu Mxra8 did not promote infection of MAYV, kudu Δ15 Mxra8 did (Figures 6G and S6F).

Ancient Origin of the Bovine Mxra8 Insertion
The Mxra8 insertion either originated once in a common ancestor of the Bos, Bubalus, and Tragelaphus lineages or up to three times independently in each of these lineages (Figures

6H and S7). Our phylogenetic reconstruction places at least 80% of the amino acid substitutions within the Mxra8 insertion along internal branches of the Bovinae tree (Figures 6H and S7A–S7C; Table S6). This indicates that the Mxra8 insertion, and the conserved amino acid substitutions within it, probably originated during the Miocene or earlier (>5.3 million years ago (5.3 mya)) (Zurano et al., 2019), before Tragelaphus diversified (Table S7). Recent, widespread introgression of the insertion appears unlikely, as the Bovinae species tree and the Mxra8 gene tree are highly congruent (Figures S7D and S7E) and the chromosome counts of Bovinae species differ substantially within and between genera (see Figure S7 and Table S8) (O'Brien, 2005).

At present, we have no evidence suggesting that alphavirus disease resistance selected for the Mxra8 insertion. Although age estimates based on nucleotide sequence divergence suggest alphaviruses evolved recently from a common ancestor (Weaver et al., 1993), RNA viruses may be considerably older than hypothesized (Zhang et al., 2018b). The insertion also could have evolved to enhance an endogenous function of Mxra8 in Bovinae physiology. As Mxra8 reportedly interacts with $\alpha_V\beta_3$ integrin and possibly other matrix proteins, the insertion might modulate its attributed roles in cell-cell adhesion, angiogenesis, and/or mesenchymal cell differentiation (Han et al., 2018; Jung et al., 2008, 2012).

The insertion in Mxra8 likely limits alphavirus infection in some Bovinae species. The mechanism of evasion is reminiscent of those postulated for mouse hepatitis virus and some arenaviruses, where alleles of the Ceacam1a or transferrin (TFR1) receptors, respectively, with sequence variations yielding lower binding affinity were selected in subsets of rodents (Demogines et al., 2013; Peng et al., 2017). Analogously, some humans are homozygous for a 32-nucleotide deletion in CCR5, which confers resistance to HIV entry (Martinson et al., 1997). Arthritogenic alphaviruses (e.g., CHIKV and RRV) failed to infect cattle and kudu cells efficiently except when an engineered variant (cattle Δmoo or kudu Δ15) but not WT Mxra8 was expressed. Moreover, introducing the "moo" insert into mouse Mxra8 produces a loss-of-function allele for CHIKV infection in vivo and phenocopies an absence of Mxra8. Consistent with this idea, four Bos taurus calves inoculated with CHIKV failed to develop viremia (Bosco-Lauth et al., 2016), and in an area of Central Africa with epidemic transmission of CHIKV, only 1 of 183 zebus had CHIKV antibodies (Guilherme et al., 1996). Similarly, in a region of New Zealand with active RRV transmission, 0 of 207 cattle were seropositive for RRV (McFadden et al., 2009), and in Australia, RRV has been isolated from horses and goats, but not cattle (Gard et al., 1988). Detailed seroepidemiological studies of Bovinae and related Bovidae species in areas of epidemic alphavirus

---

A nonsynonymous substitution occurs in the ancestor of Bovini followed by two loss events in the ancestor of Bubalina. Four more nonsynonymous substitutions occur in the ancestor of Tragelaphini. In scenario B (green symbols), where duplication of the 5-amino acid repeat unit is more common, three duplication events and a nonsynonymous substitution occur in the ancestor of Bovina. A single duplication event occurs in the Bubalina ancestor. In the ancestor of Tragelaphini, two duplication events are followed by two nonsynonymous substitutions, a duplication event, and a nonsynonymous substitution. Scenario C (purple symbols), where duplication of the 10-amino acid repeat unit is more common, is similar to scenario B with an exception in the Tragelaphini ancestor. Here, a single duplication event is followed by three nonsynonymous substitutions, a duplication event, and a nonsynonymous substitution. Scenario C also requires a single synonymous substitution in the terminal lineage leading to Tragelaphus eurycerus. A geological time scale indicating the Miocene (orange), Pliocene (yellow), and Pleistocene (light yellow) epochs is shown below.
See Figure S7 and Table S6.

transmission could clarify the relationship between exposure, infection, and resistance to disease.

Our *in vitro* and *in vivo* data suggest that animals retaining the Mxra8 insertion or those modified with an introduced insertion are resistant to infection and disease by Mxra8-dependent contemporary alphaviruses. By combining established resistance patterns of specific animals to viral infection with the sequences and structures of evolutionarily related receptor orthologs, molecular and functional analysis can elucidate how and which sequence variation alters virus-receptor interactions. Moreover, these studies may foster the development of countermeasures, as they provide a strategy for genetically modifying animals or identifying molecules that bind to specific regions of Mxra8 to promote resistance to infection by multiple alphaviruses. Indeed, small molecules that differentially bind cattle, mouse, or human Mxra8 in the region proximal to the C'-C'' loop insertion could block alphavirus attachment and infection.

STAR★METHODS

Detailed methods are provided in the online version of this paper and include the following:

- KEY RESOURCES TABLE
- LEAD CONTACT AND MATERIALS AVAILABILITY
- EXPERIMENTAL MODEL AND SUBJECT DETAILS
  - Cells and Viruses
  - Generation of Mxra8 Knockin Mice
  - Mouse Experiments
- METHOD DETAILS
  - Plasmid Construction for Trans-complementation Studies
  - Trans-complementation and Infection Experiments
  - Expression and Purification of Mxra8 Proteins
  - Protein Crystallization and X-Ray Structure Determination
  - Mxra8 ELISA Binding Assays
  - Mxra8 BLI Binding Assays
  - Virus-Cell Binding Assays
  - Sample Collection and Sequencing
  - Structural Docking Analysis
  - Whole Genome Sequence Assembly and Alignments
  - Immunoblotting
  - Evolutionary Analyses
  - Statistical Analyses
- DATA AND CODE AVAILABILITY

SUPPLEMENTAL INFORMATION

Supplemental Information can be found online at https://doi.org/10.1016/j.chom.2020.01.008.

AUTHOR CONTRIBUTIONS

A.S.K., O.Z., L.D., C.B.C., and S.C. performed the infection studies with Mxra8. O.Z., R.Z., and C.B. generated the Mxra8 genes and lentiviruses for the complementation studies. A.S.K. and K.B. performed the ELISA and BLI binding studies. A.S.K., C.A.N., K.B., and D.H.F. performed the structural analysis of mouse and cattle Mxra8 and the docking studies on CHIKV. S.L.D. provided key animal reagents. J.M.F. performed the *in vivo* studies. A.S.K., C.D., J.O., B.S., and S.A.H. analyzed the whole genome sequences and primary RNA sequences. T.W. provided the genetic analysis of the sequence insertion. M.J.L. and B.S. performed the evolutionary analysis. A.S.K., O.Z., J.M.F., and K.B. performed the data analysis. A.S.K., O.Z., M.J.L., and M.S.D. wrote the initial manuscript draft.

DECLARATION OF INTERESTS

M.S.D. is a consultant for Inbios and Emergent BioSolutions and is on the scientific advisory board of Moderna. D.H.F. is a founder of Courier Therapeutics.

REFERENCES

Adams, P.D., Afonine, P.V., Bunkóczi, G., Chen, V.B., Davis, I.W., Echols, N., Headd, J.J., Hung, L.W., Kapral, G.J., Grosse-Kunstleve, R.W., et al. (2010). PHENIX: a comprehensive Python-based system for macromolecular structure solution. Acta Crystallogr. D Biol. Crystallogr. *66*, 213–221.

Akahata, W., Yang, Z.Y., Andersen, H., Sun, S., Holdaway, H.A., Kong, W.P., Lewis, M.G., Higgs, S., Rossmann, M.G., Rao, S., et al. (2010). A virus-like particle vaccine for epidemic Chikungunya virus protects nonhuman primates against infection. Nat Med. *16*, 334–338.

Bana, N.A., Nyiri, A., Nagy, J., Frank, K., Nagy, T., Stéger, V., Schiller, M., Lakatos, P., Sugár, L., Horn, P., et al. (2018). The red deer Cervus elaphus genome CerEla1.0: sequencing, annotating, genes, and chromosomes. Mol Genet Genomics. *293*, 665–684.

Basore, K., Kim, A.S., Nelson, C.A., Zhang, R., Smith, B.K., Uranga, C., Vang, L., Cheng, M., Gross, M.L., Smith, J., et al. (2019). Cryo-EM structure of Chikungunya virus in complex with the Mxra8 receptor. Cell *177*, 1725–1737.e16.

Bosco-Lauth, A.M., Nemeth, N.M., Kohler, D.J., and Bowen, R.A. (2016). Viremia in North American mammals and birds After experimental infection with chikungunya viruses. Am. J. Trop. Med. Hyg. *94*, 504–506.

Canavez, F.C., Luche, D.D., Stothard, P., Leite, K.R., Sousa-Canavez, J.M., Plastow, G., Meidanis, J., Souza, M.A., Feijao, P., Moore, S.S., et al. (2012). Genome sequence and assembly of Bos indicus. J Hered. *103*, 342–348.

Carleton, M., Lee, H., Mulvey, M., and Brown, D.T. (1997). Role of glycoprotein PE2 in formation and maturation of the Sindbis virus spike. J. Virol. *71*, 1558–1566.

Challis, D., Antunes, L., Garrison, E., Banks, E., Evani, U.S., Muzny, D., Poplin, R., Gibbs, R.A., Marth, G., and Yu, F. (2015). The distribution and mutagenesis of short coding indels from 1,128 whole exomes. BMC Genomics *16*, 143.

Chen, V.B., Arendall, W.B., 3rd, Headd, J.J., Keedy, D.A., Immormino, R.M., Kapral, G.J., Murray, L.W., Richardson, J.S., and Richardson, D.C. (2010). MolProbity: all-atom structure validation for macromolecular crystallography. Acta Crystallogr. D Biol. Crystallogr. *66*, 12–21.

Cheng, R.H., Kuhn, R.J., Olson, N.H., Rossmann, M.G., Choi, H.K., Smith, T.J., and Baker, T.S. (1995). Nucleocapsid and glycoprotein organization in an enveloped virus. Cell *80*, 621–630.

Demogines, A., Abraham, J., Choe, H., Farzan, M., and Sawyer, S.L. (2013). Dual host-virus arms races shape an essential housekeeping protein. PLOS Biol. *11*, e1001571.

DeTulleo, L., and Kirchhausen, T. (1998). The clathrin endocytic pathway in viral infection. EMBO J. *17*, 4585–4593.

Du, X., Gertz, E.M., Wojtowicz, D., Zhabinskaya, D., Levens, D., Benham, C.J., Schäffer, A.A., and Przytycka, T.M. (2014). Potential non-B DNA regions in the human genome are associated with higher rates of nucleotide mutation and expression variation. Nucleic Acids Res. *42*, 12367–12379.

Earnest, J.T., Basore, K., Roy, V., Bailey, A.L., Wang, D., Alter, G., Fremont, D.H., and Diamond, M.S. (2019). Neutralizing antibodies against Mayaro virus require Fc effector functions for protective activity. J. Exp. Med. *216*, 2282–2301.

Edgar, R.C. (2004). MUSCLE: a multiple sequence alignment method with reduced time and space complexity. BMC Bioinformatics. *5*, 113.

Elsik, C.G., Unni, D.R., Diesh, C.M., Tayal, A., Emery, M.L., Nguyen, H.N., and Hagen, D.E. (2016). Bovine genome database: new tools for gleaning function from the Bos taurus genome. Nucleic Acids Res. *44*, D834–D839.

Emsley, P., Lohkamp, B., Scott, W.G., and Cowtan, K. (2010). Features and development of coot. Acta Crystallogr. D Biol. Crystallogr. *66*, 486–501.

Erasmus, J.H., Rossi, S.L., and Weaver, S.C. (2016). Development of vaccines for chikungunya fever. J Infect Dis. *214*, S488–S496.

Fox, J.M., Long, F., Edeling, M.A., Lin, H., van Duijl-Richter, M.K.S., Fong, R.H., Kahle, K.M., Smit, J.M., Jin, J., Simmons, G., et al. (2015). Broadly neutralizing Alphavirus antibodies bind an epitope on E2 and inhibit entry and egress. Cell *163*, 1095–1107.

Gard, G.P., Shorthose, J.E., Weir, R.P., Walsh, S.J., and Melville, L.F. (1988). Arboviruses recovered from sentinel livestock in northern Australia. Vet. Microbiol. *18*, 109–118.

Gardner, C.L., Ebel, G.D., Ryman, K.D., and Klimstra, W.B. (2011). Heparan sulfate binding by natural eastern equine encephalitis viruses promotes neuro-virulence. Proc. Natl. Acad. Sci. USA *108*, 16026–16031.

Guilherme, J.M., Gonella-Legall, C., Legall, F., Nakoume, E., and Vincent, J. (1996). Seroprevalence of five arboviruses in Zebu cattle in the Central African Republic. Trans. R. Soc. Trop. Med. Hyg. *90*, 31–33.

Han, S., Park, H.R., Lee, E.J., Jang, J.A., Han, M.S., Kim, G.W., Jeong, J.H., Choi, J.Y., Beier, F., and Jung, Y.K. (2018). Dicam promotes proliferation and maturation of chondrocyte through Indian hedgehog signaling in primary cilia. Osteoarthr. Cartil. *26*, 945–953.

Han, S.W., Jung, Y.K., Lee, E.J., Park, H.R., Kim, G.W., Jeong, J.H., Han, M.S., and Choi, J.Y. (2013). DICAM inhibits angiogenesis via suppression of AKT and p38 MAP kinase signalling. Cardiovasc. Res. *98*, 73–82.

Han, S.W., Kim, J.M., Lho, Y., Cho, H.J., Jung, Y.K., Kim, J.A., Lee, H., Lee, Y.J., and Kim, E.S. (2019). DICAM attenuates experimental colitis via stabilizing junctional complex in mucosal barrier. Inflamm. Bowel Dis. *25*, 853–861.

Hasegawa, M., Kishino, H., and Yano, T. (1985). Dating of the human-ape splitting by a molecular clock of mitochondrial DNA. J. Mol. Evol. *22*, 160–174.

Hawman, D.W., Fox, J.M., Ashbrook, A.W., May, N.A., Schroeder, K.M., Torres, R.M., Crowe, J.E., Jr., Dermody, T.S., Diamond, M.S., and Morrison, T.E. (2016). Pathogenic Chikungunya Virus Evades B Cell Responses to Establish Persistence. Cell Rep. *16*, 1326–1338.

Hayer, A., Shao, L., Chung, M., Joubert, L.M., Yang, H.W., Tsai, F.C., Bisaria, A., Betzig, E., and Meyer, T. (2016). Engulfed cadherin fingers are polarized junctional structures between collectively migrating endothelial cells. Nat Cell Biol. *18*, 1311–1323.

Heidner, H.W., Knott, T.A., and Johnston, R.E. (1996). Differential processing of Sindbis virus glycoprotein PE2 in cultured vertebrate and arthropod cells. J. Virol. *70*, 2069–2073.

Höhna, S., Landis, M.J., Heath, T.A., Boussau, B., Lartillot, N., Moore, B.R., Huelsenbeck, J.P., and Ronquist, F. (2016). RevBayes: bayesian phylogenetic inference using graphical models and an interactive model-specification language. Syst. Biol. *65*, 726–736.

Hunt, A.R., Frederickson, S., Hinkel, C., Bowdish, K.S., and Roehrig, J.T. (2006). A humanized murine monoclonal antibody protects mice either before

or after challenge with virulent Venezuelan equine encephalomyelitis virus. J. Gen. Virol. *87*, 2467–2476.

Jung, Y.K., Han, S.W., Kim, G.W., Jeong, J.H., Kim, H.J., and Choi, J.Y. (2012). DICAM inhibits osteoclast differentiation through attenuation of the integrin αVβ3 pathway. J. Bone Miner. Res. *27*, 2024–2034.

Jung, Y.K., Jeong, J.H., Ryoo, H.M., Kim, H.N., Kim, Y.J., Park, E.K., Si, H.J., Kim, S.Y., Takigawa, M., Lee, B.H., et al. (2004). Gene expression profile of human chondrocyte HCS-2/8 cell line by EST sequencing analysis. Gene *330*, 85–92.

Jung, Y.K., Jin, J.S., Jeong, J.H., Kim, H.N., Park, N.R., and Choi, J.Y. (2008). DICAM, a novel dual immunoglobulin domain containing cell adhesion molecule interacts with alphavbeta3 integrin. J. Cell. Physiol. *216*, 603–614.

Kalbfleisch, T., and Meaton, M.P. (2013). Mapping whole genome shotgun sequence and variant calling in mammalian species without their reference genomes. F1000Res. *2*, 244.

Klimstra, W.B., Ryman, K.D., and Johnston, R.E. (1998). Adaptation of Sindbis virus to BHK cells selects for use of heparan sulfate as an attachment receptor. J. Virol. *72*, 7357–7366.

Kostyuchenko, V.A., Jakana, J., Liu, X., Haddow, A.D., Aung, M., Weaver, S.C., Chiu, W., and Lok, S.M. (2011). The structure of Barmah Forest virus as revealed by cryo-electron microscopy at a 6-angstrom resolution has detailed transmembrane protein architecture and interactions. J. Virol. *85*, 9327–9333.

Lee, R.C., Hapuarachchi, H.C., Chen, K.C., Hussain, K.M., Chen, H., Low, S.L., Ng, L.C., Lin, R., Ng, M.M., and Chu, J.J. (2013). Mosquito cellular factors and functions in mediating the infectious entry of Chikungunya virus. PLoS Negl. Trop. Dis. *7*, e2050.

Lescar, J., Roussel, A., Wien, M.W., Navaza, J., Fuller, S.D., Wengler, G., Wengler, G., and Rey, F.A. (2001). The Fusion glycoprotein shell of Semliki forest virus: an icosahedral assembly primed for fusogenic activation at endosomal pH. Cell *105*, 137–148.

Li, H., and Durbin, R. (2010). Fast and accurate long-read alignment with Burrows-Wheeler transform. Bioinformatics *26*, 589–595.

Li, H., and Durbin, R. (2019). Fast and accurate short read alignment with Burrows-Wheeler transform. Bioinformatics. *25*, 1754–1760.

Maddison, W. P., and Maddison, D.R. (2019). Mesquite: a modular system for evolutionary analysis, Version 3.61. (http://www.mesquiteproject.org).

MacEachern, S., McEwan, J., and Goddard, M. (2009). Phylogenetic reconstruction and the identification of ancient polymorphism in the Bovini tribe (Bovidae, Bovinae). BMC Genomics *10*, 177.

Martinson, J.J., Chapman, N.H., Rees, D.C., Liu, Y.T., and Clegg, J.B. (1997). Global distribution of the CCR5 gene 32-basepair deletion. Nat. Genet. *16*, 100–103.

McFadden, A.M., McFadden, B.D., Mackereth, G.F., Clough, R.R., Hueston, L., Gradwell, B., and Dymond, M. (2009). A serological survey of cattle in the Thames - Coromandel district of New Zealand for antibodies to Ross river virus. N. Z. Vet. J. *57*, 116–120.

Modi, W.S., Ivanov, S., and Gallagher, D.S. (2004). Concerted evolution and higher-order repeat structure of the 1.709 (satellite IV) family in bovids. J. Mol. Evol. *58*, 460–465.

Montgomery, S.B., Goode, D.L., Kvikstad, E., Albers, C.A., Zhang, Z.D., Mu, X.J., Ananda, G., Howie, B., Karczewski, K.J., Smith, K.S., et al. (2013). The origin, evolution, and functional impact of short insertion-deletion variants identified in 179 human genomes. Genome Res. *23*, 749–761.

Mulvey, M., and Brown, D.T. (1995). Involvement of the molecular chaperone BiP in maturation of Sindbis virus envelope glycoproteins. J. Virol *69*, 1621–1627.

O'Brien, S.J. (2005). Atlas of mammalian chromosomes.

Pal, P., Dowd, K.A., Brien, J.D., Edeling, M.A., Gorlatov, S., Johnson, S., Lee, I., Akahata, W., Nabel, G.J., Richter, M.K.S., et al. (2013). Development of a highly protective combination monoclonal antibody therapy against Chikungunya virus. PLoS Pathog. *9*, e1003312.

Paredes, A.M., Brown, D.T., Rothnagel, R., Chiu, W., Schoepp, R.J., Johnston, R.E., and Prasad, B.V. (1993). Three-dimensional structure of a membrane-containing virus. Proc. Natl. Acad. Sci. USA *90*, 9095–9099.

Park, S.D., Magee, D.A., McGettigan, P.A., Teasdale, M.D., Edwards, C.J., Lohan, A.J., Murphy, A., Braud, M., Donoghue, M.T., Liu, Y., et al. (2015). Genome sequencing of the extinct Eurasian wild aurochs, Bos primigenius, illuminates the phylogeography and evolution of cattle. Genome Biol. *16*, 234.

Peng, G., Yang, Y., Pasquarella, J.R., Xu, L., Qian, Z., Holmes, K.V., and Li, F. (2017). Structural and molecular evidence suggesting coronavirus-driven evolution of mouse receptor. J. Biol. Chem. *292*, 2174–2181.

Roadmap Epigenomics Consortium, Kundaje, A., Meuleman, W., Ernst, J., Bilenky, M., Yen, A., Heravi-Moussavi, A., Kheradpour, P., Zhang, Z., Wang, J., et al. (2015). Integrative analysis of 111 reference human epigenomes. Nature *518*, 317–330.

Rose, P.P., Hanna, S.L., Spiridigliozzi, A., Wannissorn, N., Beiting, D.P., Ross, S.R., Hardy, R.W., Bambina, S.A., Heise, M.T., and Cherry, S. (2011). Natural resistance-associated macrophage protein is a cellular receptor for Sindbis virus in both insect and mammalian hosts. Cell Host Microbe *10*, 97–104.

Smith, S.A., Silva, L.A., Fox, J.M., Flyak, A.I., Kose, N., Sapparapu, G., Khomandiak, S., Ashbrook, A.W., Kahle, K.M., Fong, R.H., et al. (2015). Isolation and characterization of broad and ultrapotent human monoclonal antibodies with therapeutic activity against Chikungunya virus. Cell Host Microbe *18*, 86–95.

Smith, T.J., Cheng, R.H., Olson, N.H., Peterson, P., Chase, E., Kuhn, R.J., and Baker, T.S. (1995). Putative receptor binding sites on alphaviruses as visualized by cryoelectron microscopy. Proc. Natl. Acad. Sci. USA *92*, 10648–10652.

Song, H., Zhao, Z., Chai, Y., Jin, X., Li, C., Yuan, F., Liu, S., Gao, Z., Wang, H., Song, J., et al. (2019). Molecular basis of arthritogenic Alphavirus receptor MXRA8 binding to Chikungunya virus envelope protein. Cell *177*, 1714–1724.e12.

Strauss, J.H., Wang, K.S., Schmaljohn, A.L., Kuhn, R.J., and Strauss, E.G. (1994). Host-cell receptors for Sindbis virus. Arch. Virol. Suppl. *9*, 473–484.

Suhrbier, A., Jaffar-Bandjee, M.C., and Gasque, P. (2012). Arthritogenic alphaviruses–an overview. Nat. Rev. Rheumatol. *8*, 420–429.

Tian, X., Strassmann, J.E., and Queller, D.C. (2011). Genome nucleotide composition shapes variation in simple sequence repeats. Mol. Biol. Evol. *28*, 899–909.

Tsetsarkin, K., Higgs, S., McGee, C.E., Lamballerie, X.D., Charrel, R.N., and Vanlandingham, D.L. (2006). Infectious clones of Chikungunya virus (La Reunion isolate) for vector competence studies. Vector Borne Zoonotic Dis. *6*, 325–337.

Voss, J.E., Vaney, M.C., Duquerroy, S., Vonrhein, C., Girard-Blanc, C., Crublet, E., Thompson, A., Bricogne, G., and Rey, F.A. (2010). Glycoprotein organization of Chikungunya virus particles revealed by X-ray crystallography. Nature *468*, 709–712.

Wang, K., Lenstra, J.A., Liu, L., Hu, Q., Ma, T., Qiu, Q., and Liu, J. (2018). Incomplete lineage sorting rather than hybridization explains the inconsistent phylogeny of the wisent. Commun. Biol. *1*, 169.

Wang, K.S., Kuhn, R.J., Strauss, E.G., Ou, S., and Strauss, J.H. (1992). High-affinity laminin receptor is a receptor for Sindbis virus in mammalian cells. J. Virol. *66*, 4992–5001.

Waterhouse, A.M., Procter, J.B., Martin, D.M., Clamp, M., and Barton, G.J. (2009). Jalview, version 2–a multiple sequence alignment editor and analysis workbench. Bioinformatics *25*, 1189–1191.

Weaver, S.C., Hagenbaugh, A., Bellew, L.A., Netesov, S.V., Volchkov, V.E., Chang, G.J., Clarke, D.K., Gousset, L., Scott, T.W., and Trent, D.W. (1993). A comparison of the nucleotide sequences of eastern and western equine encephalomyelitis viruses with those of other alphaviruses and related RNA viruses. Virology *197*, 375–390.

Weaver, S.C., Powers, A.M., Brault, A.C., and Barrett, A.D. (1999). Molecular epidemiological studies of veterinary arboviral encephalitides. Vet. J. *157*, 123–138.

Weaver, S.C., Winegar, R., Manger, I.D., and Forrester, N.L. (2012). Alphaviruses: population genetics and determinants of emergence. Antiviral Res. *94*, 242–257.

Yang, Z. (1994). Maximum likelihood phylogenetic estimation from DNA sequences with variable rates over sites: approximate methods. J. Mol. Evol. *39*, 306–314.

Yang, Z. (2007). PAML 4: phylogenetic analysis by maximum likelihood. Mol Biol Evol. *24*, 1586–1591.

Yonezawa, T., Ohtsuka, A., Yoshitaka, T., Hirano, S., Nomoto, H., Yamamoto, K., and Ninomiya, Y. (2003). Limitrin, a novel immunoglobulin superfamily protein localized to glia limitans formed by astrocyte endfeet. Glia *44*, 190–204.

Zhang, R., Kim, A.S., Fox, J.M., Nair, S., Basore, K., Klimstra, W.B., Rimkunas, R., Fong, R.H., Lin, H., Poddar, S., et al. (2018a). Mxra8 is a receptor for multiple arthritogenic alphaviruses. Nature *557*, 570–574.

Zhang, R., Earnest, J.T., Kim, A.S., Winkler, E.S., Desai, P., Adams, L.J., Hu, G., Bullock, C., Gold, B., Cherry, S., et al. (2019). Expression of the Mxra8 receptor promotes Alphavirus infection and pathogenesis in mice and Drosophila. Cell Rep. *28*, 2647–2658.e5.

Zhang, W., Heil, M., Kuhn, R.J., and Baker, T.S. (2005). Heparin binding sites on Ross River virus revealed by electron cryo-microscopy. Virology *332*, 511–518.

Zhang, Y.Z., Wu, W.C., Shi, M., and Holmes, E.C. (2018b). The diversity, evolution and origins of vertebrate RNA viruses. Curr. Opin. Virol. *31*, 9–16.

Zurano, J.P., Magalhães, F.M., Asato, A.E., Silva, G., Bidau, C.J., Mesquita, D.O., and Costa, G.C. (2019). Cetartiodactyla: updating a time-calibrated molecular phylogeny. Mol. Phylogenet. Evol. *133*, 256–262.

STAR★METHODS

KEY RESOURCES TABLE

REAGENT or RESOURCE	SOURCE	IDENTIFIER
Antibodies		
Anti-Mxra8 mAb 1G11.E6	Zhang et al., 2018a	N/A
Anti-Mxra8 mAb 1H1.F5	Zhang et al., 2018a	N/A
Anti-Mxra8 mAb 3G2.F5	Zhang et al., 2018a	N/A
Anti-Mxra8 mAb 4E7.D10	Zhang et al., 2018a	N/A
Anti-Mxra8 mAb 7F1.D8	Zhang et al., 2018a	N/A
Anti-Mxra8 mAb 8F7.E1	Zhang et al., 2018a	N/A
Anti-Mxra8 mAb 9G2.D6	Zhang et al., 2018a	N/A
CHK-11	Pal et al., 2013	N/A
CHK-48	Pal et al., 2013	N/A
CHK-84	Pal et al., 2013	N/A
CHK-124	Pal et al., 2013	N/A
CHK-152	Pal et al., 2013	N/A
CHK-166	Pal et al., 2013	N/A
CHK-265	Pal et al., 2013	N/A
1I9	Smith et al., 2015	N/A
3B4C-4	Hunt et al., 2006	N/A
MAYV-115 N297Q	Earnest et al., 2019	N/A
MAYV-134 N297Q	Earnest et al., 2019	N/A
Alexa Fluor 488 conjugated goat anti-mouse IgG	Thermo Fisher	A28175; RRID: AB_2536161
Alexa Fluor 647 conjugated goat anti-Armenian hamster IgG	Abcam	ab173004; RRID: AB_2732023
Alexa Fluor 647 conjugated goat anti-mouse IgG	Thermo Fisher	A21235; RRID: AB_2535804
Alexa Fluor 647 conjugated goat anti-human IgG	Thermo Fisher	A21445; RRID: AB_2535862
Peroxidase conjugated goat anti-mouse IgG (H + L)	Jackson ImmunoResearch	115-035-062; RRID: AB_2338504
Peroxidase conjugated goat anti-Armenian hamster IgG (H + L)	Jackson ImmunoResearch	127-035-160; RRID: AB_2338976
Bacterial and Virus Strains		
Chikungunya virus (strain 181/25)	Erasmus et al., 2016	GenBank: AF192908
Chikungunya virus (strain AF15561)	Hawman et al., 2016	GenBank: EF452493
Chikungunya virus (strain LR-2006)	Tsetsarkin et al., 2006	GenBank: KY575571
Mayaro virus (strain BeH407)	World Reference Center for Emerging Viruses and Arboviruses	GenBank: AAY45742
Ross River virus (strain T48)	World Reference Center for Emerging Viruses and Arboviruses	GenBank: ACV67002
O'nyong'nyong virus (strain MP30)	World Reference Center for Emerging Viruses and Arboviruses	GenBank: AAC97207
Venezuelan equine encephalitis virus (strain TC-83)	World Reference Center for Emerging Viruses and Arboviruses	GenBank: L01443
Biological Samples		
Muscle tissue, *Bos Taurus*	Whole Foods Market	N/A
Liver tissue, *Bos javanicus*	Saint Louis Zoo	ISIS #108161
Muscle tissue, *Bos grunniens*	The Yak Boys	YB105

(*Continued on next page*)

Continued

REAGENT or RESOURCE	SOURCE	IDENTIFIER
Muscle tissue, *Bison bison*	Whole Foods Market	N/A
Muscle tissue, *Bubalus bubalis*	Nicky Farms	4695
Liver tissue, *Tragelaphus eurycerus*	Saint Louis Zoo	ISIS #103656
Liver tissue, *Tragelaphus angasii*	Saint Louis Zoo	ISIS #118494
Muscle and liver tissue, *Tragelaphus imberbis*	Saint Louis Zoo	ISIS #107129
Liver tissue, *Muntiacus muntjac*	Saint Louis Zoo	ISIS #103117
Muscle tissue, *Odocoileus virginianus*	Case Farms	N/A
Chemicals, Peptides, and Recombinant Proteins		
Chikungunya virus-like particles (strain 37997)	Akahata et al., 2010	N/A
Mouse Mxra8 ectodomain$_{23-296}$	Basore et al., 2019	N/A
Mouse +moo Mxra8 ectodomain	This study	N/A
Mouse +5 Mxra8 ectodomain	This study	N/A
Mouse +8 Mxra8 ctodomain	This study	N/A
Mouse +9 Mxra8 ectodomain	This study	N/A
Mouse +10 Mxra8 ectodomain	This study	N/A
Mouse +[GGS]$_5$ Mxra8 ectodomain	This study	N/A
Cattle Mxra8 ectodomain$_{24-309}$	This study	N/A
Cattle Δmoo Mxra8 ectodomain	This study	N/A
Mouse Mxra8 fused to mouse IgG2b Fc region	Zhang et al., 2018	N/A
Mouse +moo Mxra8 fused to mouse IgG2b Fc region	This study	N/A
Mouse +8 Mxra8 fused to mouse IgG2b Fc region	This study	N/A
Mouse +10 Mxra8 fused to mouse IgG2b Fc region	This study	N/A
Mouse +[GGS]$_5$ Mxra8 fused to mouse IgG2b Fc region	This study	N/A
Cattle Mxra8 fused to mouse IgG2b Fc region	This study	N/A
Cattle Δmoo Mxra8 fused to mouse IgG2b Fc region	This study	N/A
Buffalo Mxra8 fused to mouse IgG2b Fc region	This study	N/A
Buffalo Δ5 Mxra8 fused to mouse IgG2b Fc region	This study	N/A
Kudu Mxra8 fused to mouse IgG2b Fc region	This study	N/A
Kudu Δ15 Mxra8 fused to mouse IgG2b Fc region	This study	N/A
Critical Commercial Assays		
TaqMan RNA-to-Ct 1-Step Kit	Thermo Fisher	4392939
In-Fusion HD Cloning Plus	Takara	638910
HiScribe T7 *In Vitro* Transcription Kit	New England BioLabs	E2040S
MEGAclear Transcription Clean-Up Kit	Thermo Fisher	AM1908
Deposited Data		
X-ray crystal structure of murine Mxra8	Basore et al., 2019	PDB: 6NK3
Electron Cryo-Microscopy of Chikungunya VLP in complex with mouse Mxra8 receptor	Basore et al., 2019	PDB: 6NK6; EMD-9394
Crystal Structure of *Bos taurus* Mxra8 Ectodomain	This study	PDB: 6ORT
Bos primigenius isolate:CPC98 Raw sequence reads	Park et al., 2015	BioProject: PRJNA294709; SRR2465682
Bos indicus strain:Nelore RefSeq Genome sequencing	Canavez et al., 2012	BioProject: PRJNA360096; XM_019976191
Bos javanicus WGS data	Kalbfleisch and Meaton, 2013	BioProject: PRJNA325061; SRR4035276
Bos grunniens WGS data	N/A	BioProject: PRJNA359997; SRR5140177
Bubalus bubalis assembly	N/A	BioProject: PRJNA207334; AWWX01000000
Syncerus caffer paired end sequencing	N/A	BioProject: PRJNA341313; SRR4104498
Tragelaphus angasii RNA-seq data	N/A	BioProject: PRJNA388863; SRR5647659
Ovis vignei paired end sequencing	N/A	BioProject: PRJEB5463; ERR454948
Pseudois nayaur genome sequencing and assembly	N/A	BioProject: PRJNA361448; SRR5439716

(Continued on next page)

REAGENT or RESOURCE	SOURCE	IDENTIFIER
Capra ibex paired end sequencing	N/A	BioProject: PRJNA361447; SRR5260693
Moschus berezovskii raw sequence reads	N/A	BioProject: PRJNA289641; SRR2098995
Cervus elaphus genome sequencing and assembly	Bana et al., 2018	BioProject: PRJNA324173; SRR4013902
Experimental Models: Cell Lines		
NIH/3T3	ATCC	CRL-1658; RRID: CVCL_0594
HEK-293	ATCC	CRL-1573; RRID: CVCL_0045
Vero	ATCC	CCL-81; RRID: CVCL_0059
Bos taurus corneal endothelial cells	ATCC	CRL-2048; RRID: CVCL_2865
Expi293F	Thermo Fisher	A14527
C57BL/6J primary MEF	This study	N/A
C57BL/6J Mxra8$^{WT/KO}$ primary MEF	This study	N/A
C57BL/6J Mxra8$^{KO/KO}$ primary MEF	Zhang et al., 2019	N/A
C57BL/6J Mxra8$^{moo/KO}$ primary MEF	This study	N/A
C57BL/6J Mxra8$^{moo/moo}$ primary MEF	This study	N/A
Bos gaurus primary fibroblasts	Modi et al., 2004	N/A
Syncerus caffer primary fibroblasts	Modi et al., 2004	N/A
Boselaphus tragelaphus primary fibroblasts	Modi et al., 2004	N/A
Tragelaphus imberbis primary fibroblasts	Modi et al., 2004	N/A
Experimental Models: Organisms/Strains		
Mouse: C57BL/6J	Jackson Laboratory	000664; RRID: IMSR_JAX:000664
Mouse: C57BL/6J Mxra8$^{WT/KO}$	This study	N/A
Mouse: C57BL/6J Mxra8$^{KO/KO}$	This study	N/A
Mouse: C57BL/6J Mxra8$^{moo/KO}$	This study	N/A
Mouse: C57BL/6J Mxra8$^{moo/moo}$	This study	N/A
Oligonucleotides		
Mxra8 sgRNA-1: 5'-CTTGTGGATATGTATTCGGCNGG-3'	Genome Engineering and iPSC Center, Washington University School of Medicine	N/A
Mxra8 sgRNA-2: 5'ACTTGTGGATATGTATTCGGNGG-3'	Genome Engineering and iPSC Center, Washington University School of Medicine	N/A
CHIKV-AF FOR: 5'-TCGACGCGCCATCTTTAA-3'	Zhang et al., 2019	N/A
CHIKV-AF REV: 5'-ATCGAATGCACCGCACACT-3'	Zhang et al., 2019	N/A
CHIKV-AF Probe: 5'-/56-FAM/ACCAGCCTG/ZEN/CACCCACTCCTCAGAC/3IABkFQ/-3'	Zhang et al., 2019	N/A
See Table S5 for primer sequences and annealing temperatures used to amplify *Mxra8* from primary tissue samples of different animals		N/A
Recombinant DNA		
pLV-EF1a vector	Hayer et al., 2016	Addgene 85132; RRID: Addgene_85132
Codon-optimized mouse Mxra8 cloned into pLV-EF1a vector	Zhang et al., 2018a	GenBank: NM_024263
Codon-optimized mouse +moo Mxra8 cloned into pLV-EF1a vector	This study	N/A
Codon-optimized cattle (*Bos taurus*) Mxra8 cloned into pLV-EF1a vector	This study	GenBank: NM_001075830
Codon-optimized cattle Δmoo Mxra8 cloned into pLV-EF1a vector	This study	N/A
Codon-optimized zebu (*Bos indicus*) Mxra8 cloned into pLV-EF1a vector	This study	GenBank: XM_019976191
Codon-optimized zebu Δmoo Mxra8 cloned into pLV-EF1a vector	This study	N/A

(Continued on next page)

Continued

REAGENT or RESOURCE	SOURCE	IDENTIFIER
Codon-optimized water buffalo (*Bubalus bubalis*) Mxra8 cloned into pLV-EF1a vector	This study	GenBank: XM_006066948.2
Codon-optimized water buffalo Δ5 Mxra8 cloned into pLV-EF1a vector	This study	N/A
Codon-optimized lesser kudu (*Tragelaphus angasii*) Mxra8 cloned into pLV-EF1a vector	This study	N/A
Codon-optimized lesser kudu Δ15 Mxra8 cloned into pLV-EF1a vector	This study	N/A
Codon-optimized goat (*Capra hircus*) Mxra8 cloned into pLV-EF1a vector	This study	GenBank: XM_018060531
Codon-optimized dog (*Canis lupus familiaris*) Mxra8 cloned into pLV-EF1a vector	This study	GenBank: XM_546712
Codon-optimized rat (*Rattus norvegicus*) Mxra8 cloned into pLV-EF1a vector	This study	GenBank: NM_001007002
Codon-optimized chimp (*Pan troglodytes*) Mxra8 cloned into pLV-EF1a vector	This study	GenBank: NM_001280245
Codon-optimized horse (*Equus caballus*) Mxra8 cloned into pLV-EF1a vector	This study	GenBank: XM_023636045
Codon-optimized sheep (*Ovis aries*) Mxra8 cloned into pLV-EF1a vector	This study	GenBank: XM_027975805
Codon-optimized turkey (*Meleagris gallopavo*) Mxra8 cloned into pLV-EF1a vector	This study	GenBank: XP_010721105.1
Codon-optimized duck (*Anas platyrhynchos*) Mxra8 cloned into pLV-EF1a vector	This study	GenBank: XM_027443263
Codon-optimized chicken (*Gallus gallus*) Mxra8 cloned into pLV-EF1a vector	This study	GenBank: NP_989967
psPAX2	Didier Trono	Addgene 12260; RRID: Addgene_12260
pMD2.G	Didier Trono	Addgene 12259; RRID: Addgene_12259
Codon-optimized mouse Mxra8 ectodomain$_{23-296}$ cloned into pET21a vector	Basore et al., 2019	N/A
Codon-optimized mouse Mxra8 +5 ectodomain cloned into pET21a vector	This study	N/A
Codon-optimized mouse Mxra8 +8 ectodomain cloned into pET21a vector	This study	N/A
Codon-optimized mouse Mxra8 +9 ectodomain cloned into pET21a vector	This study	N/A
Codon-optimized mouse Mxra8 +10 ectodomain cloned into pET21a vector	This study	N/A
Codon-optimized mouse Mxra8 +[GGS]$_5$ ectodomain cloned into pET21a vector	This study	N/A
Codon-optimized cattle Mxra8 ectodomain$_{24-309}$ cloned into pET21a vector	This study	GenBank: NM_001075830
Codon-optimized cattle Δmoo ectodomain Mxra8 cloned into pET21a vector	This study	N/A
Codon optimized mouse Mxra8 ectodomain and mouse IgG2b Fc region cloned into pCDNA3.4 vector	This study	N/A
Codon optimized mouse +moo Mxra8 ectodomain and mouse IgG2b Fc region cloned into pCDNA3.4 vector	This study	N/A
Codon optimized mouse +8 Mxra8 ectodomain and mouse IgG2b Fc region cloned into pCDNA3.4 vector	This study	N/A
Codon optimized mouse +10 Mxra8 ectodomain and mouse IgG2b Fc region cloned into pCDNA3.4 vector	This study	N/A
Codon optimized mouse +[GGS]$_5$ ectodomain Mxra8 and mouse IgG2b Fc region cloned into pCDNA3.4 vector	This study	N/A

Continued

REAGENT or RESOURCE	SOURCE	IDENTIFIER
Codon optimized cattle Mxra8 ectodomain and mouse IgG2b Fc region cloned into pCDNA3.4 vector	This study	N/A
Codon optimized cattle Δmoo Mxra8 ectodomain and mouse IgG2b Fc region cloned into pCDNA3.4 vector	This study	N/A
Codon optimized buffalo Mxra8 ectodomain and mouse IgG2b Fc region cloned into pCDNA3.4 vector	This study	N/A
Codon optimized buffalo Δ5 Mxra8 ectodomain and mouse IgG2b Fc region cloned into pCDNA3.4 vector	This study	N/A
Codon optimized kudu Mxra8 ectodomain and mouse IgG2b Fc region cloned into pCDNA3.4 vector	This study	N/A
Codon optimized kudu Δ15 Mxra8 ectodomain and mouse IgG2b Fc region cloned into pCDNA3.4 vector	This study	N/A
Software and Algorithms		
Burrows-Wheeler Aligner	Li and Durbin, 2019	http://bio-bwa.sourceforge.net/
MUSCLE	Edgar, 2004	https://www.ebi.ac.uk/Tools/msa/muscle/
RevBayes	Höhna et al., 2016	https://revbayes.github.io/
Mesquite	Maddison and Maddison, 2019	https://www.mesquiteproject.org/
PAML	Yang, 2007	http://abacus.gene.ucl.ac.uk/software/paml.html
FigTree	Andrew Rambaut	http://tree.bio.ed.ac.uk/software/figtree/; Version 1.4.4
FlowJo	FlowJo, LLC	Versions 9 and 10
PyMOL	Schrodinger	Version 2.1.0
UCSF Chimera	RVBI	https://www.cgl.ucsf.edu/chimera/; Version 1.13
GraphPad Prism	GraphPad	Version 8.2.1
Other		
Evolution analysis scripts and sequence alignments	This study	https://github.com/mlandis/mxra8_bovinae

LEAD CONTACT AND MATERIALS AVAILABILITY

Further information and requests for resources and reagents should be directed to and will be fulfilled by the Lead Contact author Michael S. Diamond (diamond@wusm.wustl.edu). All plasmids, antibodies, cells, viruses, and mouse lines developed for this study are available under Material Transfer Agreements from Washington University School of Medicine.

EXPERIMENTAL MODEL AND SUBJECT DETAILS

Cells and Viruses

NIH-3T3, HEK-293, and Vero cells were obtained from ATCC and were cultured at 37°C in DMEM supplemented with 10% fetal bovine serum (Hyclone), 100 U/ml penicillin, 100 μg/ml streptomycin, and 10 mM HEPES. *Bos taurus* corneal endothelial cells (CRL-2048) were obtained from the ATCC and were cultured at 37°C in DMEM supplemented with 20% fetal bovine serum (Hyclone), 100 U/ml penicillin, 100 μg/ml streptomycin, and 10 mM HEPES. Expi293 cells were obtained from Thermo Fisher and cultured shaking at 37°C and 8% CO_2 in Expi293 Expression Medium. Primary MEFs were generated from embryos obtained on E13. The head and internal organs were dissected from the embryos, washed, minced in the presence of 0.05% trypsin-EDTA, and cultured until confluency. Primary kudu (*Tragelaphus imberbis*) fibroblasts (generously provided by T. Raudsepp and J. Womack, Texas A&M University) were maintained in DMEM supplemented with 20% fetal bovine serum (Hyclone), 100 U/ml penicillin, 100 mg/ml streptomycin, and 10 mM HEPES.. The following alphaviruses were propagated in Vero cells and titered by focus forming assay as described previously (Fox et al., 2015): CHIKV 181/25, CHIKV AF15561, MAYV (BeH407), RRV (T48), ONNV (MP30), and VEEV-GFP (TC-83).

Generation of Mxra8 Knockin Mice

All mouse studies were performed after approval by the Institutional Animal Care and Use Committee at the Washington University School of Medicine and the Saint Louis Zoo (Assurance number A3381-01). Gene-edited Mxra8 mice were generated with support

from the Genome Engineering and iPSC center and Department of Pathology Micro-Injection Core (Washington University School of Medicine). The 45-nucleotide "moo" insertion sequence (GGCGAGCAGCGCGTGGGCGAGCAGCGCTTGGGCGAGCAGCGCGTG) from cattle Mxra8 was inserted into exon 3 of mouse Mxra8. Two sgRNAs were selected based on a low off-target profile and distance to target site: sgRNA-1: 5'-CTTGTGGATATGTATTCGGCNGG-3' and sgRNA-2: 5'ACTTGTGGATATGTATTCGGNGG-3'. The two gRNAs were synthesized *in vitro* (HiScribe T7 *In Vitro* Transcription Kit, New England BioLabs) and purified (MEGAclear Transcription Clean-Up Kit, Thermo Fisher). Guide RNAs, Cas9 protein, and the oligo donor sequence modified with silent blocks (gtccactgggacctcagcgggggcccgggcagccaacggcgccgacttgtggatatgtatAGTgcgGGCGAGCAGCGCGTGGGCGAGCAGCGC TTGGGCGAGCAGCGCGTGGggtgaacagcgcgtgtacgagccgcgcgatcgcgaccgcctcctgctgtcgccttctgct) were complexed and electroporated into C57BL/6 zygotes. After microinjection, founder lines were confirmed by genotyping and next-generation sequencing.

Mouse Experiments

Four-week-old congenic *Mxra8*[WT/WT], *Mxra8*[WT/KO], *Mxra8*[KO/KO], *Mxra8*[moo/KO], *Mxra8*[moo/moo] male or female C57BL/6J mice were inoculated subcutaneously in the footpad with 10^3 FFU of CHIKV AF15561 strain. The *Mxra8*[KO/KO] (out of frame 8 nucleotide deletion) were generated by CRISPR-Cas9 editing and characterized previously (Zhang et al., 2019). At 3 days post infection, mice were euthanized, perfused extensively with PBS, and serum and tissues were collected. Foot swelling (width x height) was monitored using digital calipers as previously described. RNA was extracted from serum and tissues using the MagMax-96 Viral RNA Isolation Kit (Thermo Fisher). Viral RNA levels were quantified by qRT-PCR using a TaqMan RNA-to-Ct 1-Step Kit (Thermo Fisher), compared to a CHIKV RNA standard curve, and expressed on a $\log_{10}$ scale as viral focus-forming unit (FFU) equivalents per gram of tissue or milliliter of serum. Primers and probes used are as follows: CHIKV-AF FOR: 5'-TCGACGCGCCATCTTTAA-3'; CHIKV-AF REV: 5'-ATCGAATGCACCGCACACT-3'; CHIKV-AF Probe: 5'-/56-FAM/ACCAGCCTG/ZEN/CACCCACTCCTCAGAC/3IABkFQ/-3'.

METHOD DETAILS

Plasmid Construction for Trans-complementation Studies

Mxra8 cDNA fragments containing a C-terminal FLAG tag were codon-optimized, synthesized, and inserted into the lentivirus vector pLV-EF1a using an In-Fusion HD Cloning Kit (Takara) for the following species: *Mus musculus* (Genbank accession no. NM_024263), *Bos taurus* (NM_001075830), *Bos indicus* (XM_019976191), *Bubalus bubalis* (XM_006066948.2), *Tragelaphus angasii* (primary sequence, see Table S4), *Capra hircus* (XM_018060531), *Canis lupus familiaris* (XM_546712), *Rattus norvegicus* (NM_001007002), *Pan troglodytes* (NM_001280245), *Equus caballus* (XM_023636045), *Ovis aries* (XM_027975805), *Meleagris gallopavo* (XP_010721105.1), *Anas platyrhynchos* (XM_027443263), and *Gallus gallus* (NP_989967). The mouse Mxra8 + moo was generated by inserting residues "GEQRVGEQRLGEQRV" after amino acid residue 98. The cattle Δmoo, zebu Δmoo, and kudu Δ15 Mxra8 were generated by removing residues 96-110. The Bubalus Δ5 was generated by removing residues 96-100. All sequences were codon-optimized. Plasmids were transformed into One Shot Stbl3 Chemically Competent *E. coli* (Thermo Fisher) and bacteria were grown at 30°C on LB Agar plates with carbenicillin (100 μg/ml). Colonies were picked and grown overnight at 30°C in LB supplemented with carbenicillin (100 μg/ml). Plasmids were extracted (Qiagen) and sequenced using the following primers: GCACT TGATGTAATTCTCCTTGGAATTTGC, CTCAAGCCTCAGACAGTGGTTCAAAGT and GGTGGAAAATAACATATAGACAAACGCAC. The following primers were used to sequence the following species: *Bos indicus*: GTCTATGAGCCTAGGGACCGA and GTCTAT GAGCCTAGGGACCGA; *Bubalus bubalis*: CGCGTATACGAGCCTCGA and ATAGAGTCGCAGTTGAGGCAG; *Tragelaphus angasii*: TGGGGAAAGACGGGCCT; *Equus caballus*: CGATCGAGGTCGACTGCTTC and ACAGAGTTGCCGTAGCTGTAG; *Gallus gallus*: CAGGGGAGGATACTGATGCC and TGGGCCCCTCTTTATCCGA; *Meleagris gallopavo*: ATGCTTTTACAGATGGTAACTTCAG and TGAACATCACTGATACTGCCTTTG; and *Anas platyrhynchos*: TCAGGGGAGAATATTTATGCCACAA and TGAATATAACCGAT ACTGCTTTCGC.

Trans-complementation and Infection Experiments

Lentiviruses were packaged with psPAX2 (Addgene #12260) and pMD2.G (Addgene #12259) vectors in HEK-293 cells using FugeneHD (Promega). *ΔMxra8* 3T3 cells (Zhang et al., 2018a) were transduced with lentiviruses and selected with blasticidin for 7 days. Surface expression of Mxra8 was assessed by flow cytometry after staining with a pool of seven hamster anti-mouse Mxra8 mAbs (Zhang et al., 2018a) (1 μg/ml for all species except for dog Mxra8 [10 μg/ml]), and Alexa Fluor 647 conjugated goat anti-Armenian hamster IgG (1 μg/ml) at 4°C. Surface expression of avian Mxra8 orthologs was assessed using a FLAG tag located at the N-terminus located downstream of the signal peptide sequence. Mouse Mxra8 expression levels were compared to *ΔMxra8* 3T3 (negative) and wild-type 3T3 (positive) cells. Mxra8 surface expression levels of all other species were compared to *ΔMxra8* 3T3 (negative) and *ΔMxra8* 3T3 cells transduced with mouse Mxra8 (positive). Trans-complemented *ΔMxra8* 3T3 cells with Mxra8 surface expression levels of less than 90% after blasticidin selection were further enriched by fluorescence activated cell sorting. Cells (2.5×10^5) were incubated with a pool of anti-Mxra8 mAbs (1G11.E6, 1H1.F5, 3G2.F5, 4E7.D10, 7F1.D8, 8F7.E1, and 9G2.D6) (1 μg/ml) in 1% BSA/PBS for 30 min at 4°C. After 30 min, cells were washed and incubated with Alexa Fluor 647 conjugated goat anti-hamster IgG (1 μg/ml). After a 30-min incubation, cells were washed, resuspended in PBS supplemented with 2% FBS and 1 mM EDTA, and sorted using a BD FACSAria II. Cells positive for Mxra8 expression subsequently were expanded in culture.

Trans-complemented *ΔMxra8* 3T3 cells were inoculated with CHIKV 181/25 (MOI 3, 9.5 h), CHIKV AF15561 (MOI 3, 9.5 h), MAYV (MOI 3, 24 h), RRV (MOI 3, 32 h), or VEEV (MOI 3, 12 h) in DMEM supplemented with 2% FBS. At indicated time points, cells were

harvested, fixed and permeabilized using Foxp3 Transcription Factor Staining Buffer Set (Thermo Fisher), and stained for viral antigen after incubation with the following antibodies: CHIKV (mouse mAb CHK-11 (Pal et al., 2013)), MAYV (mouse mAb CHK-48 (Fox et al., 2015)), RRV (human mAb 1I9 (Smith et al., 2015)), or VEEV (mouse 3B4C-4 (Hunt et al., 2006)). Cells were washed, incubated with Alexa Fluor 647 conjugated goat anti-mouse IgG or goat anti-human IgG (Thermo Fisher), and analyzed by flow cytometry using a MACSQuant Analyzer 10 (Miltenyi Biotec). For multi-step growth curves, trans-complemented ΔMxra8 3T3 cells or primary MEFs were inoculated (MOI 0.01) with CHIKV 181/25, CHIKV AF15561, or CHIKV LR-2006 for 1 h, washed, and maintained in 2% FBS growth medium. Viral supernatants were harvested at indicated timepoints, titered on Vero cells, fixed, permeabilized, and stained with CHK-11 and horseradish peroxidase-conjugated goat anti-mouse IgG. Infected foci were visualized using TrueBlue peroxidase substrate (KPL) and quantitated on an ImmunoSpot 5.0.37 Macroanalyzer (Cellular Technologies).

Bovine cornea cells were transduced with lentiviruses and selected with blasticidin for 7 days. Mxra8 surface expression was confirmed by flow cytometry as described above. To generate a clonal line that expressed high levels of Mxra8, bovine cornea cells were subjected to fluorescence-activated cell sorting as described above. Bovine cornea cells were inoculated with CHIKV 181/25 (MOI 3, 12 h) or RRV (MOI 3, 12 h) in 5% FBS growth medium. After infection, cells were harvested, fixed, permeabilized, stained with virus-specific antibodies, and analyzed by flow cytometry.

Primary kudu fibroblasts were transduced with lentiviruses encoding kudu or kudu Δ15 Mxra8. Cell surface expression of Mxra8 was confirmed using a pool of anti-Mxra8 mAbs. Cells with >90% Mxra8 surface expression were inoculated with MAYV (MOI 3, 26 h). After infection, cells were harvested, fixed, permeabilized, stained with biotinylated anti-MAYV antibodies (MAYV-115 and MAYV-134) (Earnest et al., 2019) that contain an N297Q mutation in the Fc region, and analyzed by flow cytometry.

Expression and Purification of Mxra8 Proteins
A cDNA fragment encoding residues 24-309 of the *Bos taurus* Mxra8 extracellular domain was codon-optimized, synthesized, and inserted into the pET21a vector using the NdeI/NotI sites. After sequence confirmation, the plasmid construct was transformed into BL21(DE3) chemically competent cells (Thermo Fisher). Cells were grown at 37°C to an optimal density (600 nm) of 0.8 and induced with 0.1 mM IPTG for 4 h. Cells were harvested and resuspended in 50 mM Tris-HCl, 1 mM EDTA, 0.01% NaN_3, 1 mM DTT, 25% sucrose (TENDS) buffer, and lysed in 50 mM Tris-HCl, 1 mM EDTA, 0.01% NaN_3, 1 mM DTT, 200 mM sodium chloride, 1% sodium deoxycholate and 1% Triton X-100. Inclusion bodies were isolated from the cellular lysate after centrifugation at 6,000 x g for 20 min and washed in TENDS buffer supplemented with 100 mM NaCl and 0.5% Triton X-100. A final wash was performed in the same buffer without 0.5% Triton X-100. Inclusion bodies were denatured in in 100 mM Tris-HCl, 6 M guanidinium chloride and 20 mM β-mercaptoethanol for 1 h. Denatured protein was oxidatively refolded overnight at 4°C in 400 mM L-arginine, 100 mM Tris-HCl, 5 mM reduced glutathione, 0.5 mM oxidized glutathione, 10 mM EDTA and 200 mM phenylmethylsulphonyl fluoride. Refolded protein was concentrated using a 10,000-molecular weight cut-off stirred cell concentrator (EMD Millipore). Concentrated protein was further purified by HiLoad 16/600 Superdex 75 size exclusion chromatography (GE Healthcare) and HiTrap Q HP anion exchange chromatography (GE Healthcare). Purity and oligomeric state were confirmed by SDS-PAGE analysis and size exclusion chromatography coupled with multi-angle light scattering.

The mouse Mxra8-Fc fusion protein was generated as previously described where a cDNA fragment encoding Mxra8 (Genbank accession no. NM_024263) and the mouse IgG2b Fc region was synthesized (Integrated DNA Technologies) and inserted into the pCDNA3.4 vector. The mouse +moo Mxra8-Fc, mouse-Mxra8+8-Fc, mouse-Mxra8+10-Fc, and mouse +(GGS)₅ proteins were generated as described above with the addition of the amino acids "GEQRVGEQRLGEQRV", "QRVGEQRL", "GEQRVGEQRL", or "(GGS)₅" after amino acid residue 98, respectively. Cattle (Genbank accession no. NM_001075830, residues 24-358), cattle Δmoo (Genbank accession no. NM_001075830, residues 24-95 and 111-358), Bubalus (residues 24-348), Bubalus Δmoo (residues 24-95, 101-348), kudu (residues 24-358), and kudu Δ15 (residues 24-95, 111-358) Mxra8-Fc proteins were generated as described above. Mxra8-Fc plasmids were diluted in Opti-MEM, incubated with HYPE-5 reagent (OZ Biosciences), and the complex was transfected into Expi-293 cells (Thermo Fisher, 10⁶ cells/ml). Cells were supplemented daily with Expi293 medium and 2% (w/v) Hyclone Cell Boost. Four days post transfection, the supernatant was harvested by centrifuging at 3,000 x g for 15 min and purified using Protein A Sepharose 4B (Thermo Fisher). After elution, Mxra8-Fc proteins were dialyzed into 20 mM HEPES, 150 mM NaCl, pH 7.5 and stored at -80°C. Purity was confirmed by SDS-PAGE analysis.

Protein Crystallization and X-Ray Structure Determination
Purified, recombinant *Bos taurus* Mxra8 protein (residues 24-309) produced in *E. coli* was crystallized by hanging drop vapor diffusion at 15 mg/ml in 0.1 M HEPES, pH 8.0, 6% (w/v) PEG 6000, and 1.0 M $LiCl_2$. Crystals were cryo-protected in the mother liquor supplemented with 25% ethylene glycol and flash-cooled in liquid nitrogen. Diffraction data was collected at the Advanced Light Source MBC Beamline 4.2.2 (100K; 1.0000 Å wavelength) and processed with XDS. Four datasets were collected by translating along a single crystal. Datasets were processed and merged using XDS. Initial phases were obtained through molecular replacement with Phaser using murine Mxra8 coordinates (PDB 6NK3) as a search model. Model building was carried out in COOT (Emsley et al., 2010) and refinement was performed with Phenix (Adams et al., 2010). The overall electron density of the structure was good except in regions corresponding to amino acid residues 79-85 and 95-112, where weak electron density was noted and building of well-restrained geometric models was challenging. For these two regions, refinement was carried out with occupancy values set to 0.5. The final *Bos taurus* Mxra8 model contains mature residues 33-309 and 117 water molecules with an R_{work} of 21.8% and R_{free}

of 24.2%. Data collection and refinement statistics are reported in Table S2. Structural validation was assessed using Molprobity (Chen et al., 2010), and structural figures were generated using PyMOL (Schrodinger, Version 2.1.0).

Mxra8 ELISA Binding Assays
Maxisorp ELISA plates were coated with anti-CHIKV mAb 4N12 (Smith et al., 2015) (2 μg/ml) overnight in sodium bicarbonate buffer, pH 9.3. Plates were washed four times with PBS and blocked with 4% BSA for 1 h at 25°C. CHIKV VLPs were diluted to 1 μg/ml in 2% BSA and added for 1 h at 25°C. Mxra8-Fc proteins were diluted in 2% BSA and incubated for 1 h at 25°C. Plates were washed with PBS and incubated with horseradish peroxide conjugated goat anti-mouse IgG (H + L) (1:2000 dilution, Jackson ImmunoResearch) for 1 h at 25°C. After washing, plates were developed with 3,3'-5,5' tetramethylbenzidine substrate (Thermo Fisher) and 2N H_2SO_4. Plates were read at 450 nM using a TriStar Microplate Reader (Berthold). Anti-Mxra8 mAb ELISAs were performed by coating Maxisorp ELISA plates with Mxra8-Fc proteins (2 μg/ml) overnight in sodium bicarbonate buffer, pH 9.3. Plates were washed four times with PBS and 0.05% Tween-20 and blocked with 4% BSA for 1 h at 25°C. Anti-Mxra8 mAbs were diluted in 2% BSA and added for 1 h at 25°C. Plates were washed with PBS and 0.05% Tween-20 and incubated with horseradish peroxidase conjugated goat anti-Armenian hamster IgG (H + L) (1:2000 dilution, Jackson ImmunoResearch) for 1 h at 25°C. After washing, plates were developed and read as described above.

Mxra8 BLI Binding Assays
BLI experiments were performed in 10 mM HEPES (pH 7.4), 150 mM NaCl, 3 mM EDTA, and 0.005% P20 surfactant with 1% BSA at 25°C using an Octet RED96 (ForteBio). CHK-265 was biotinylated as previously described (Fox et al., 2015), loaded onto streptavidin biosensors (ForteBio) until saturation, then incubated with CHIKV VLP for 5 min. To measure the affinity of mouse and cattle Δmoo Mxra8 to CHIKV VLP, the loaded streptavidin biosensors were dipped into increasing concentrations of Mxra8 protein (10 nM to 1 μM) for 5 min, followed by a 5 min dissociation. Recombinant cattle and mouse + moo Mxra8 proteins (5 μM) were allowed to associate and dissociate for 5 min at each step. Real-time data was analyzed using BIAevaluation 3.1 (GE Healthcare) and kinetic curves and steady-state equilibrium were fitted using a global 1:1 binding algorithm with drifting baseline.

Virus-Cell Binding Assays
ΔMxra8 3T3 cells or trans-complemented cells (3 x 10^4 cells) were incubated with CHIKV 181/25 (MOI 200) for 1 h at 4°C. Cells were washed extensively with cold PBS, and viral antigen staining was performed using a cocktail of CHIKV anti-E1 and anti-E2 antibodies (mAbs CHK-11, CHK-84, CHK-124, and CHK-166 (Pal et al., 2013)). Cells were washed, incubated with Alexa Fluor 647 conjugated goat anti-mouse IgG (Thermo Fisher), and analyzed by flow cytometry.

Sample Collection and Sequencing
All experiments were performed after approval by the Institutional Animal Care and Use Committee at the Washington University School of Medicine and the Saint Louis Zoo (Assurance number A3381-01). Muscle and liver samples were obtained from banked samples collected at necropsy. All sample sources are listed in Table S4. Total RNA was extracted using TRIzol and a Direct-zol RNA kit (Zymo Research). First strand cDNA was generated using a SuperScript III First-Strand Synthesis System (Thermo Fisher). Species- and gene-specific primers were designed from deposited sequences and assembled whole genome sequences (Tables S4 and S5). PCR master mixes were prepared in a nucleic acid-free PCR workstation. Bovinae Mxra8 genes were amplified using nested PCR with 1X Q5 Reaction Buffer, 200 μM dNTPs, 200 nM Forward primer, 200 nM Reverse primer, 2 μl cDNA, 1X Q5 High GC Enhancer, and 1 μl of Q5 High-Fidelity DNA Polymerase (NEB). The following amplification protocol was used for both first- and second-round amplifications: 1) 98°C for 30 sec; 2) 98°C for 20 sec; 3) 60-68°C for 30 sec; 4) 72°C for 60 sec; 5) 72°C for 2 min; with steps 2-4 repeated for 35 cycles. All primer sequences and annealing temperatures are listed in Table S5. PCR products were separated on a 1% agarose gel, and the band of the predicted size was purified by gel-extraction (Qiagen). Purified PCR products were sequenced using amplification primers and primers that target a conserved region in the *Mxra8* gene (TGCCACCTGCACCACCACTAC and GTAGTGGTGGTGCAGGTGGCA).

Structural Docking Analysis
The cattle Mxra8 crystal structure (PDB 6ORT) was superimposed onto the Mxra8 chains in the 1) Mxra8-bound CHIKV-VLP cryo-EM model (PDB 6NK6 and (Basore et al., 2019)) using the MatchMaker tool in USCF Chimera and 2) MXRA8-bound CHIKV p62-E1 glycoprotein crystal structure (PDB 6JO8) using the 'super' command in PyMOL (Version 2.1.0, Schrodinger).

Whole Genome Sequence Assembly and Alignments
Whole genome sequences of the species listed in Table S4 were aligned to the *Bos taurus* genome (Elsik et al., 2016) using BWA-MEM from the Burrows-Wheeler Aligner (Li and Durbin, 2010) to look for reads mapping to the *Mxra8* gene and the ''GEQRVGEQRL GEQRV'' insertion sequence. For non-Bovinae species, reads were mapped to genomes with either a 15-residue insertion (*Bos taurus*), partial insertion (*Bubalus bubalis*; AWWX01000000), no insertion (*Ovis aries*; CM008472) to identify reads overlapping the insert junction. *Mxra8* nucleotide sequences were aligned with MUSCLE. Quality for alignments was refined by manual assessment and adjustment of misaligned sites.

Immunoblotting

Primary MEFs (10^6 cells) were harvested and lysed in RIPA buffer (Thermo Fisher) containing a protease inhibitor cocktail (Roche). Cell lysates were mixed with LDS buffer (Thermo Fisher), incubated at 70°C for 10 min, and electrophoresed using 10% Bis-Tris gels (Thermo Fisher) in MOPS running buffer. Separated proteins were transferred to a PVDF membrane using an iBlot2 Dry Blotting System (Thermo Fisher). The PVDF membrane was blocked with 5% non-fat milk, probed with hamster anti-Mxra8 mAbs (3G2.F5 or 9G2.D6, 1 μg/ml) and horseradish peroxidase conjugated goat anti-Armenian hamster IgG, and developed with SuperSignal West Pico Chemiluminescent Substrate (Thermo Fisher).

Evolutionary Analyses

Phylogenetic analyses were executed in RevBayes (Höhna et al., 2016). The unrooted *Mxra8* gene tree topology was estimated under the HKY+Gamma substitution model (Hasegawa et al., 1985; Yang, 1994) (see Figure S7 and Table S6).

Statistical Analyses

Statistical significance was assigned using Prism Version 8 (GraphPad) when $p < 0.05$. Statistical analysis of viral infection levels was determined by one-way ANOVA with Dunnett's post-test. Statistical analysis of *in vivo* experiments was determined by either one-way or two-way ANOVA with a Kruskal-Wallis or Dunnett's post-test depending on the data distribution and the number of comparison groups. The statistical tests, number of independent experiments, and number of experimental replicates are indicated in the Figure legends.

DATA AND CODE AVAILABILITY

The authors declare that all data supporting the findings of this study are available within the paper. Analysis scripts and the sequence alignment are available at: https://github.com/mlandis/mxra8_bovinae. The X-ray crystal structure of cattle Mxra8 has been deposited as PDB 6ORT.

Supplemental Information

An Evolutionary Insertion in the Mxra8

Receptor-Binding Site Confers Resistance

to Alphavirus Infection and Pathogenesis

Arthur S. Kim, Ofer Zimmerman, Julie M. Fox, Christopher A. Nelson, Katherine Basore, Rong Zhang, Lorellin Durnell, Chandni Desai, Christopher Bullock, Sharon L. Deem, Jonas Oppenheimer, Beth Shapiro, Ting Wang, Sara Cherry, Carolyn B. Coyne, Scott A. Handley, Michael J. Landis, Daved H. Fremont, and Michael S. Diamond
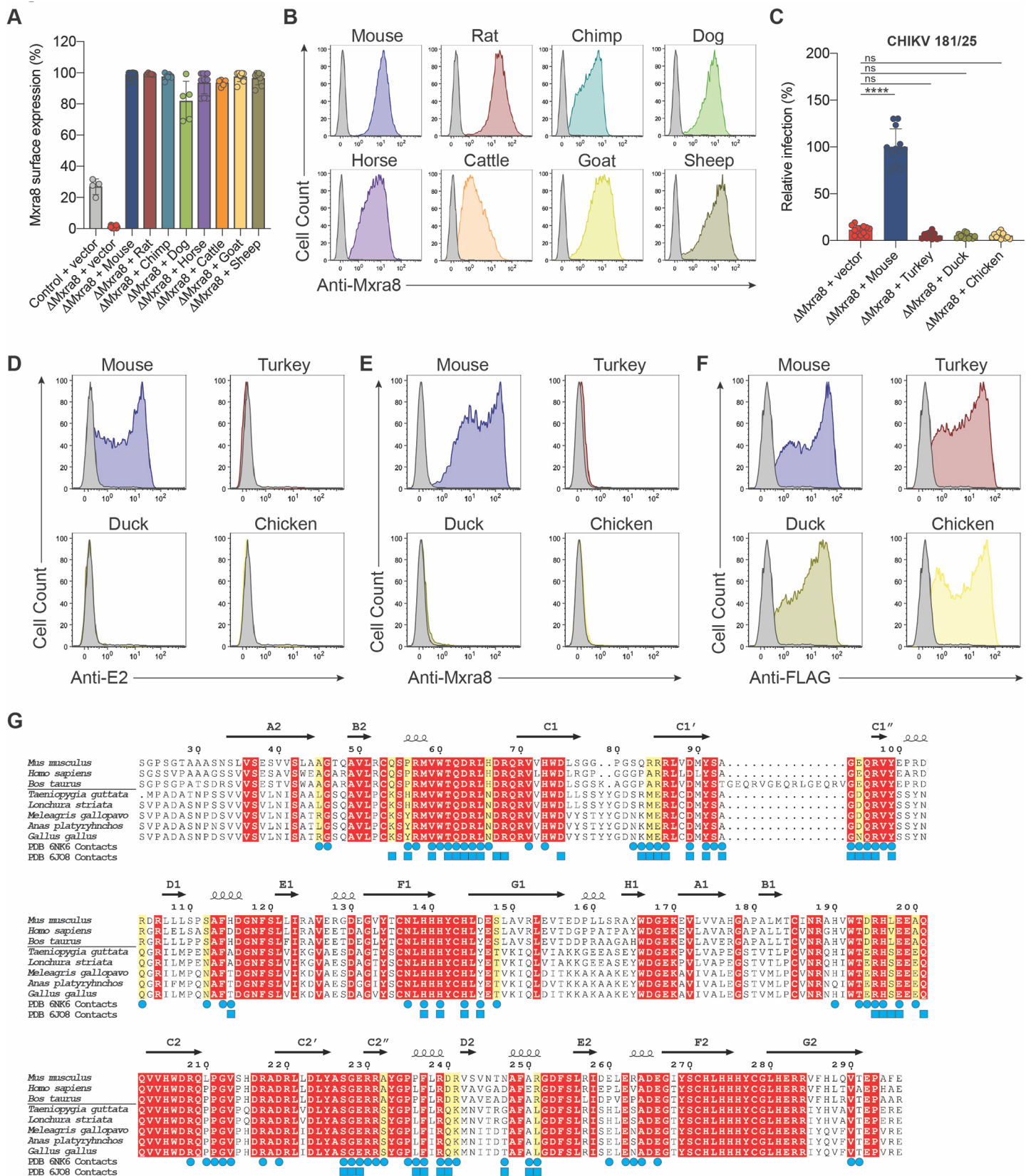
Figure S1. Expression and infection of mammalian and avian Mxra8 orthologs in Δ*Mxra8* 3T3 cells, Related to Figure 1. Data are pooled from two to ten experiments (n = 4 to 18 replicates) (**A**) and representative flow cytometry plots (**B**) showing cell surface expression of mouse, rat, chimpanzee, dog, horse, cattle, goat, and sheep Mxra8 after lentivirus trans-complementation of Δ*Mxra8* 3T3 cells and staining with species cross-reactive anti-Mxra8 mAbs. **C-D**. Lentivirus complementation of Δ*Mxra8* 3T3 with Mxra8 cDNA from mouse, turkey, duck, or chicken. Cells were inoculated with CHIKV (181/25) and analyzed by staining with anti-E2 mAbs. Data

are from four experiments (n = 12 replicates; one-way ANOVA with Dunnett's post-test: ****, $P < 0.0001$). **E-F**. Representative flow cytometry plots showing Mxra8 surface expression of mouse, turkey, duck, and chicken Mxra8 with (**E**) a pool of anti-Mxra8 mAbs or (**F**) anti-FLAG mAb. **G.** Structure-based alignment of mouse (*Mus musculus*), human, (*Homo sapiens*), cattle (*Bos taurus*), zebra finch (*Taeniopygia guttata*), striated finch (*Lonchura striata*), turkey (*Meleagris gallopavo*), duck (*Anas platyrhynchos*), and chicken (*Gallus gallus*) using ALINE; finches can act as amplifying hosts for some encephalitic (*e.g.*, WEEV) but not arthritogenic alphaviruses. The black line in the species names indicates grouping of mammals (*top*) and birds (*bottom*). Red boxes indicate conserved residues, white boxes indicate non-conserved residues, and yellow boxes indicate CHIKV contact residues that are conserved differently in mammals or birds. Secondary structure was assigned using DSSP and indicated above the sequence. Blue circles and blue squares represent mouse Mxra8 (PDB 6NK6) and human MXRA8 (PDB 6JO8) contact residues (>50% buried surface area) with the CHIKV E2-E1 heterodimer, respectively (Basore et al., 2019; Song et al., 2019).
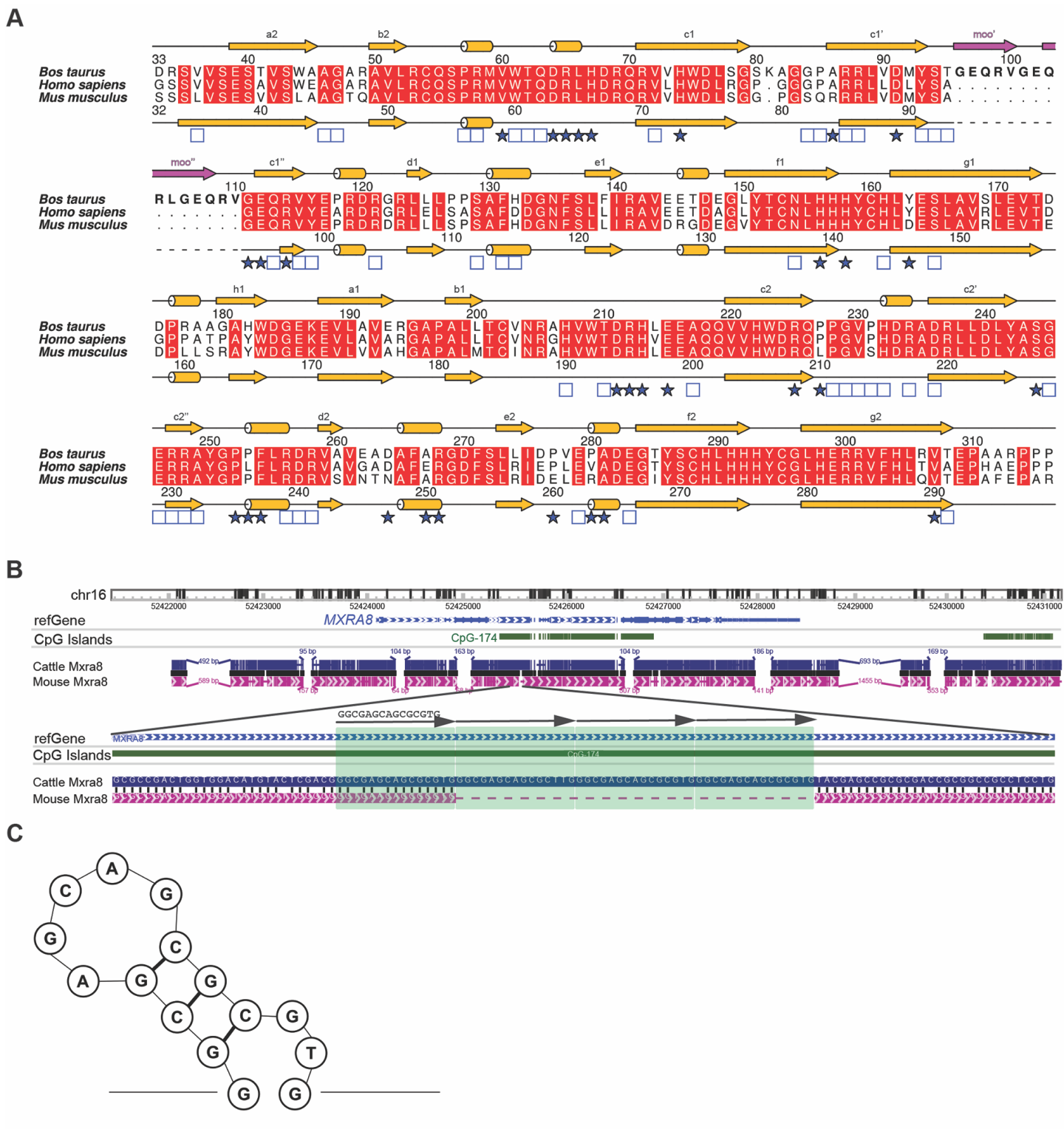
Figure S2. Sequence alignments and analysis of Mxra8, Related to Figure 2. A. Structure-based alignment of mouse, human, and cattle Mxra8 using ALINE. Red boxes indicate conserved residues and white boxes indicated non-conserved residues. Secondary structure was assigned using the DSSP algorithm and is shown in yellow for cattle (top) and mouse (bottom). The β-strands are labeled above the mouse secondary structure according to standard convention. The 15-amino acid cattle Mxra8 insertion is indicated in magenta. The symbols below the alignment indicate mouse Mxra8 contact residues with the CHIKV E2-E1 heterodimer (PDB 6NK6) as calculated by PDBePISA. Open boxes represent 10-40% buried surface area and stars represent 50-90% buried surface area as defined previously (Basore et al., 2019). **B**. Genome comparison of the cattle (blue) and mouse (magenta) Mxra8 gene using Washington University Epigenome Browser (https://epigenomegateway.wustl.edu). Predicted CpG islands are indicated in dark green. The primary 15-nucleotide sequence and the three copies of

the 15-nucleotide tandem repeat insertion are highlighted in green in the bottom panel. **C**. Predicted DNA secondary structure of cattle Mxra8 amino acids [111]GEQRV[115] shows the formation of a DNA loop in the sense strand of the double stranded DNA. DNA secondary structure was generated using mfold (Zuker, 2003). During cell replication, polymerase slippage and subsequent reattachment may cause a bubble, or a single-stranded DNA, to form in the newly synthesized strand. Slippage is thought to occur in sections of DNA with tandem repeat patterns, such as those in the *Mxra8* gene. The single stranded DNA repeat is predicted to form a stem-loop structure, which potentially increases the likelihood of formation and stabilization of a bubble. DNA repair mechanisms subsequently realign the template with the new strand resulting in the straightening and removal of the bubble. Thus, DNA polymerase slippage can cause the newly created DNA strand to contain an expanded section, such as the 45-nucleotide insertion in cattle *Mxra8*.

A

MW (kDa)

250
150
100
75
50
37
25
20
15
10

NR   R

UV Absorbance
400
300
200
100
0

Volume (ml)
0   20   40   60   80   100

B

MW (kDa)

250
150
100
75
50
37
25
20
15
10

NR   R

UV Absorbance
300
200
100
0

Volume (ml)
0   20   40   60   80   100

C

D1

H   180   183   188
A   193
G   173   149   162   157
F
C   80   71
C'   86   93
C''   115   112   108
m'   96   100
m''   108   103
Moo
D   119   121
E   140   138
B   198   200

n   39   45
A

D2

B   53   50
E   273   275
D   260   259
G   297   308
F   292   284
C   220   226
C'   242   236
C''   247   249
c

D

MW (kDa)

Mouse | Mouse + moo | Cattle | Cattle Δmoo   Mouse | Mouse + moo | Cattle | Cattle Δmoo

250
150
100
75
50
37
25
20
15
10

Non-reduced   Reduced

E

Mouse

OD$_{450}$
3
2
1
0

Concentration [μg/ml]
0.01   0.1   1   10

Mouse + moo

OD$_{450}$
3
2
1
0

Concentration [μg/ml]
0.01   0.1   1   10

Cattle

OD$_{450}$
3
2
1
0

Concentration [μg/ml]
0.01   0.1   1   10

Cattle Δmoo

OD$_{450}$
3
2
1
0

Concentration [μg/ml]
0.01   0.1   1   10

3G2.F5
4E7.D10
8F7.E1
9G2.D6
Isotype

F

Mouse

BLI signal (nm)
1.0
0.8
0.6
0.4
0.2
0.0

1000 nM
500 nM
100 nM
50 nM

Time (s)
0   100   200   300   400

Cattle Δmoo

BLI signal (nm)
1.0
0.8
0.6
0.4
0.2
0.0

1000 nM
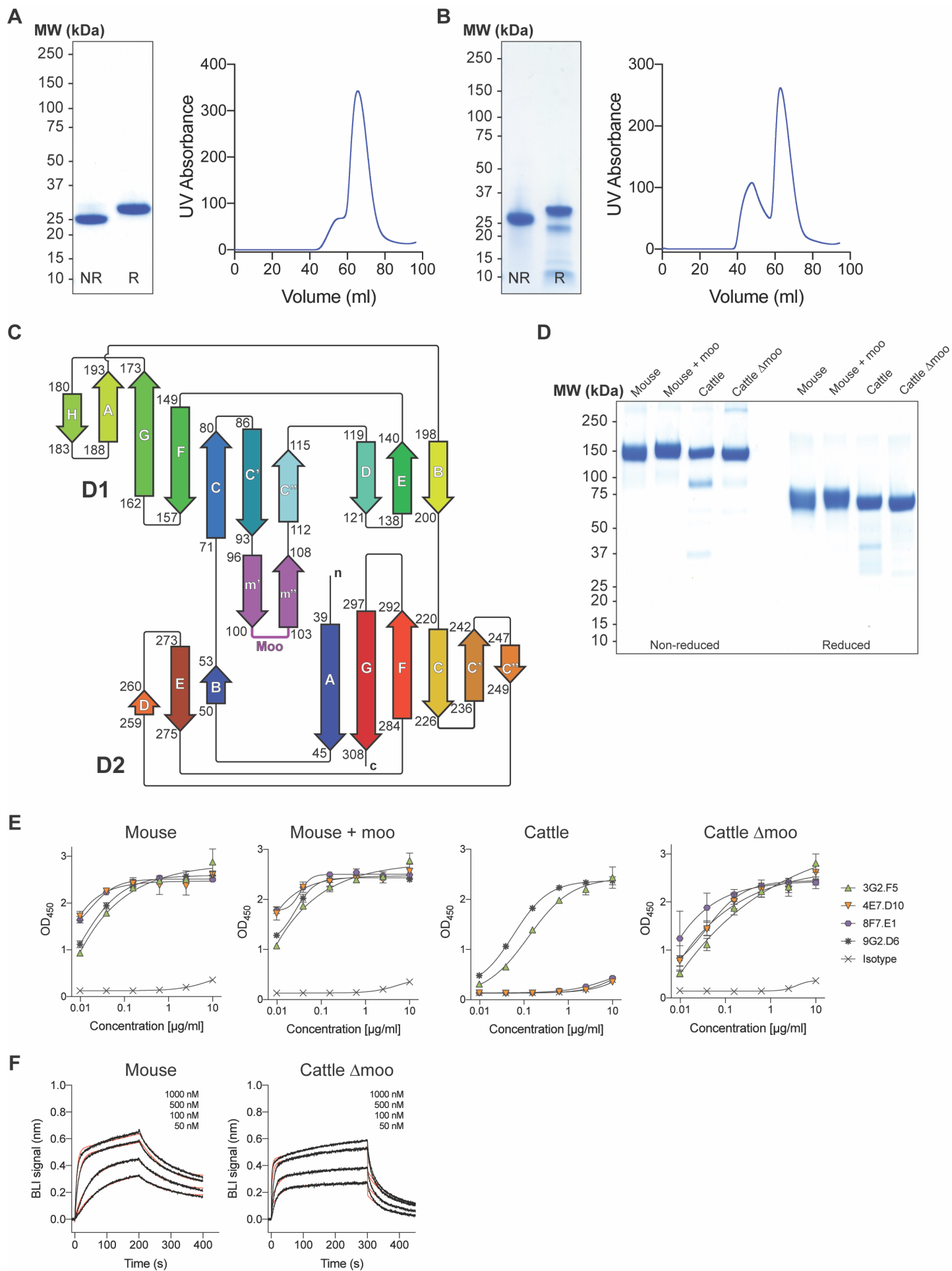500 nM
100 nM
50 nM

Time (s)
0   100   200   300   400

Figure S3. Purification and structural topology of mouse and cattle Mxra8 protein variants, Related to Figures 2 and 3. A-B. Mxra8 ectodomain of (**A**) mouse or (**B**) cattle was expressed in bacteria, oxidatively refolded, and purified by size exclusion chromatography. (*Left*) Coomassie-stained SDS-PAGE of refolded mouse Mxra8 under non-reducing and reducing conditions. (*Right*) Size exclusion chromatography profile of Mxra8 proteins. **C**. Topology diagram of cattle Mxra8. The β-strands of each Ig domain are labeled according to standard convention. The 15-residue 'moo' insertion is colored purple and forms β-strands (moo' [m'] and moo'' [m'']). The two Ig domains are labeled D1 and D2. The N- and C-termini of the Mxra8 protein are labeled in lowercase. **D**. Coomassie-stained SDS-PAGE of mouse, mouse + moo, cattle, and cattle Δmoo Mxra8-Fc proteins under non-reducing and reducing conditions. **E.** Binding of increasing concentrations of anti-Mxra8 mAbs 3G2.F5, 4E7.D10, 8F7.E1, 9G2.D6, and isotype control mAb to adsorbed mouse, mouse + moo, cattle, and cattle Δmoo Mxra8-Fc fusion proteins by ELISA. Data are pooled from four experiments performed in duplicate. **F.** Kinetic sensograms of mouse (left) and cattle Δmoo (right) Mxra8 binding to CHIKV VLPs fit to a 1:1 binding model. Raw experimental traces (1000, 500, 100, and 50 nM) are shown in black, and fit traces are shown in red. Data are representative of three (cattle Δmoo) to six (mouse) experiments.
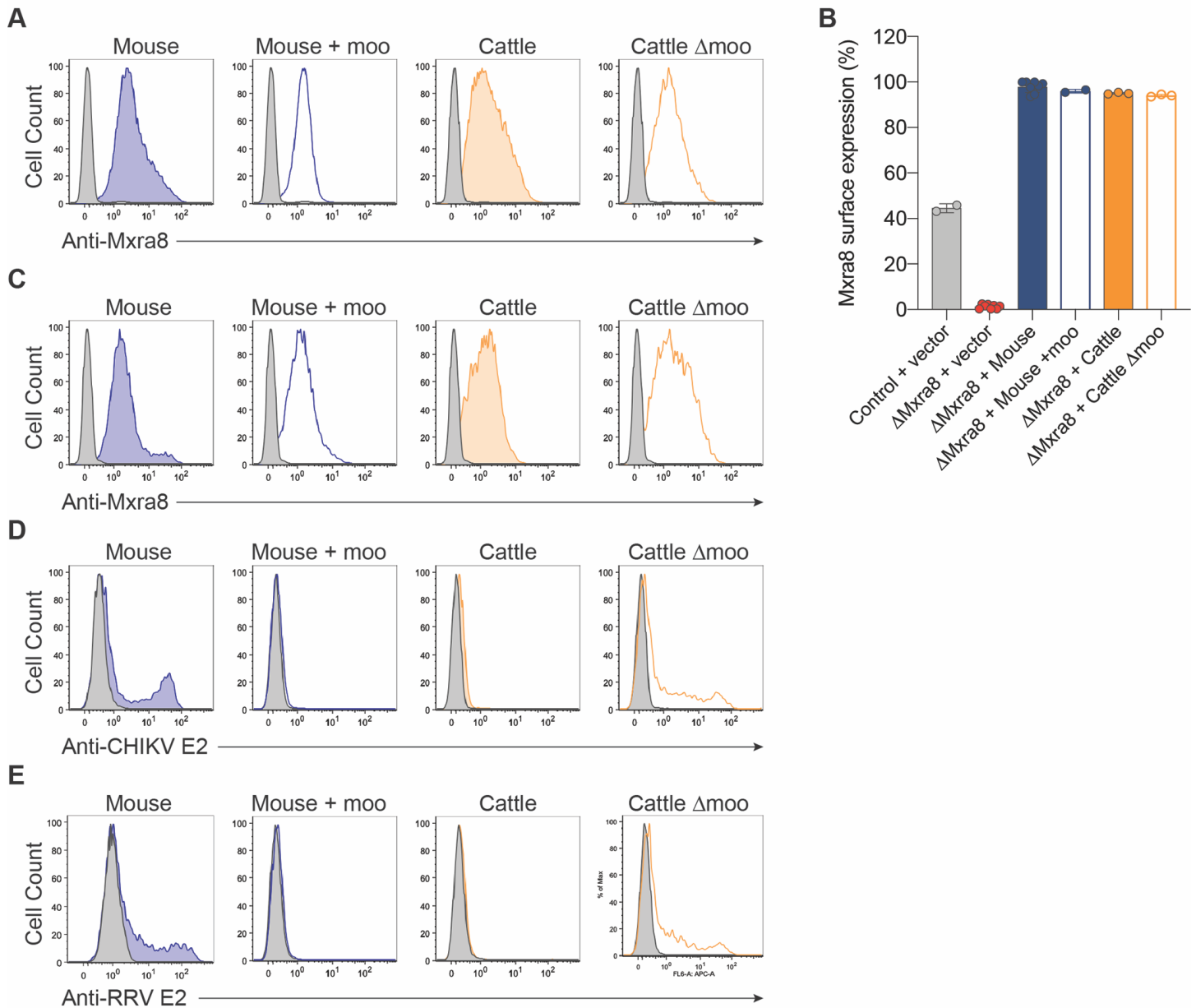
Figure S4. Expression of mouse and cattle Mxra8 variants on the surface of Δ*Mxra8* 3T3 cells and bovine cells, Related to Figure 3. A. 3T3 ΔMxra8 cells were complemented with empty vector, mouse, mouse + moo, cattle or cattle Δmoo Mxra8 and stained for Mxra8 surface expression using a pool of anti-Mxra8 mAbs. **B**. Representative flow cytometry histograms showing cell surface expression of mouse, mouse + moo, cattle, and cattle Δmoo Mxra8 variants. Data are representative of three experiments. **C.** Flow cytometry histograms showing cell surface expression of mouse, mouse + moo, cattle, and cattle Δmoo Mxra8 variants after lentivirus complementation of bovine corneal cells using a pool of anti-Mxra8 mAbs. Data are representative of three experiments. Histograms for wild-type bovine corneal cells are shown in gray. **D-E**. Flow cytometry histograms showing (**D**) CHIKV or (**E**) RRV infection of cow cells complemented with mouse, mouse + moo, cattle, and cattle Δmoo Mxra8 gene variants. Histograms for wild-type bovine corneal cells are shown in gray. Data are representative of three experiments.
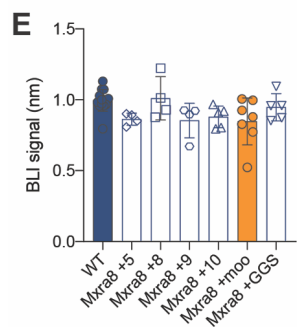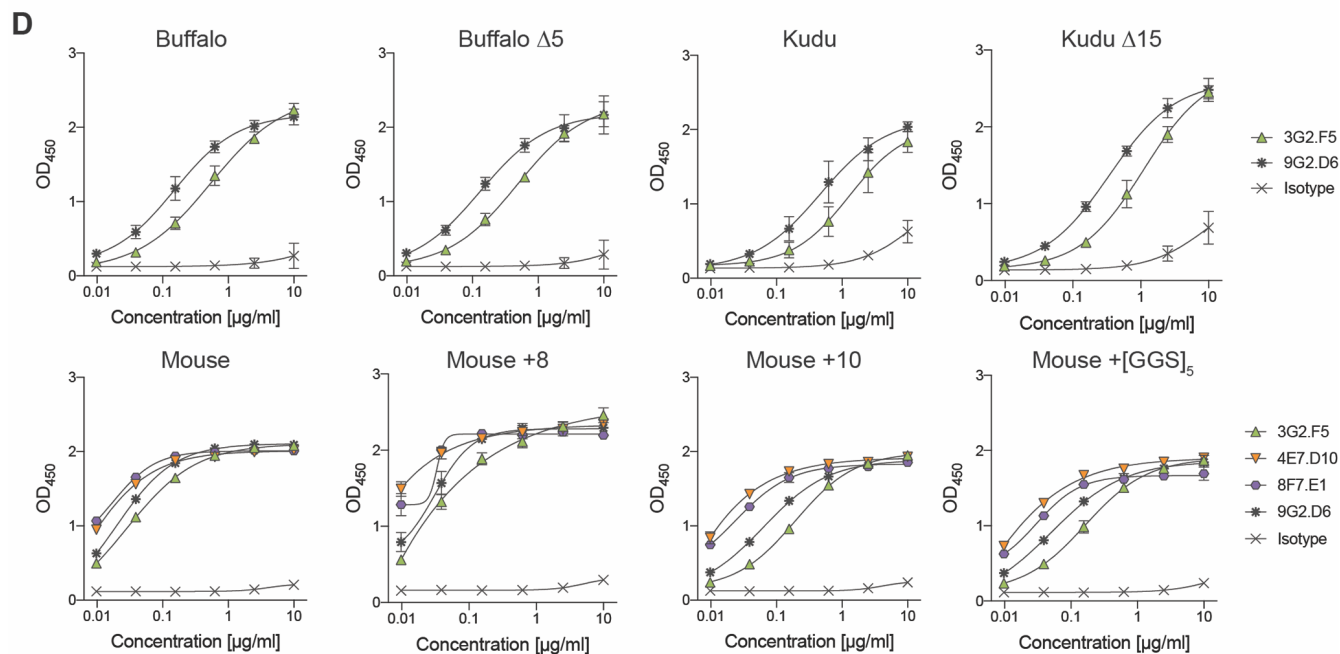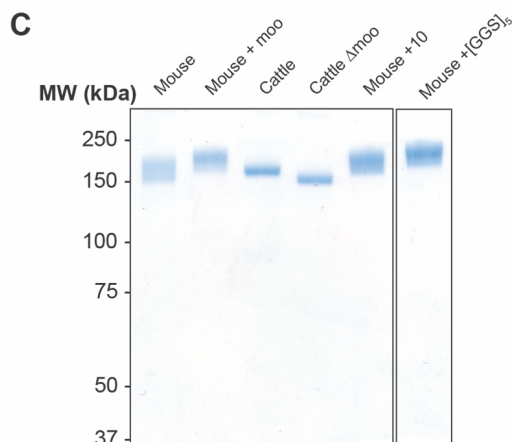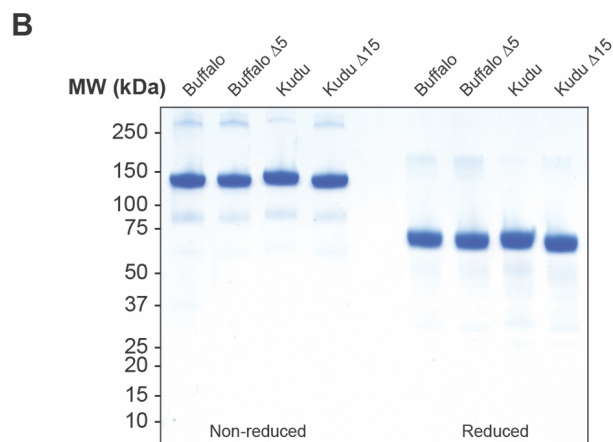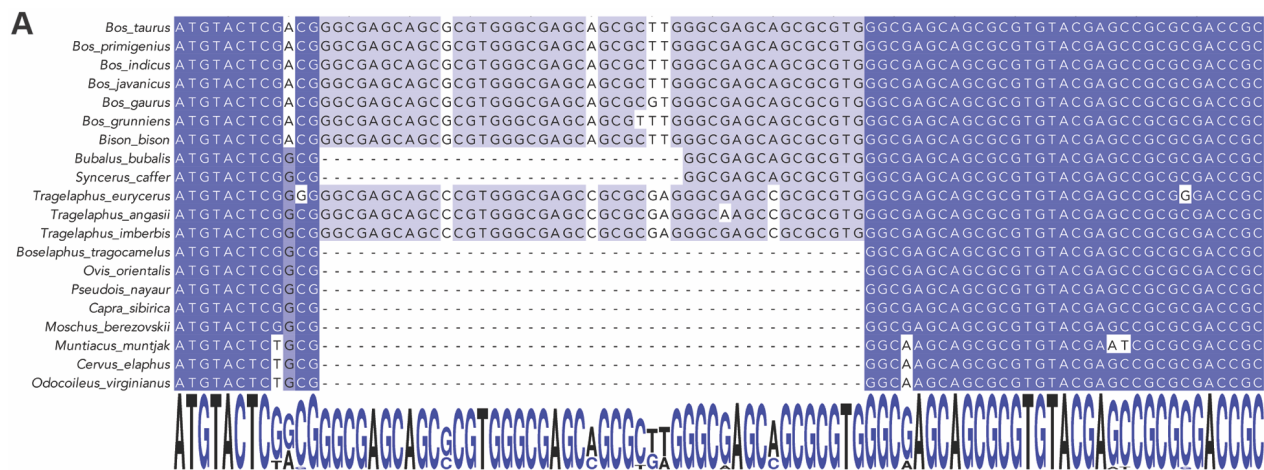
Figure S5. Expression and antigenic characterization of water buffalo, kudu, and mouse Mxra8-Fc protein variants, Related to Figures 5 and 6. A. Nucleotide sequence alignments of *Mxra8* sequences from Bovidae, Moschidae, and Cervidae family members in the region of the insertion site in D1. The sequences were obtained after assembly of deposited sequences (**Table S4**) or extraction of mRNA and primary sequencing (**Table S5** and **STAR Methods**), aligned using MUSCLE, and visualized using Jalview. Nucleotide consensus plot was generated using WebLogo3. For species with both types of data, we used sequencing from tissue samples as primary data and WGS data as confirmation. Five versions of the Mxra8 alignment were generated: (1) the complete alignment contains all sites for all species; (2) the trimmed alignment is identical to the complete alignment, but removes all sites following the first stop codon (*Bos taurus* genomic coordinates 16:51,173,039 – 51,176,528); (3) the no-insertion alignment contains all sites from the trimmed alignment except for the 45 nucleotide insertion for a total of 1344 nucleotides [*Bos taurus* 45-nucleotide insertion genomic coordinates 16:51,173,324 – 51,173,368]; (4) the insertion alignment includes only the 45-nucleotide Bovinae insertion plus the GEQRV repeat unit conserved across all mammals for a total of 60 nucleotides (*Bos taurus* insertion + GEQRV genomic coordinates 16:51,173,324 – 51,173,383); and (5) the insertion + flank alignment includes the same sites as the insertion alignment plus two 30-nucleotide flanking regions for a total of 120 nucleotides (*Bos taurus* insertion + flank genomic coordinates 16:51,173,294 – 51,173,413). **B**. Coomassie-stained SDS-PAGE of water buffalo, water buffalo Δ5, kudu, and kudu Δ15 Mxra8-Fc proteins under non-reducing and reducing conditions. **C**. Coomassie-stained SDS-PAGE of mouse, mouse + moo, cattle, cattle Δmoo, mouse +10, and mouse+[GGS]$_5$ Mxra8-Fc proteins under non-reducing conditions. **D.** Binding of increasing concentrations of anti-Mxra8 mAbs 3G2.F5, 9G2.D6, and isotype control to adsorbed water buffalo, water buffalo Δ5, kudu, kudu Δ15, mouse, mouse +8, mouse +10, and mouse +[GGS]$_5$ Mxra8-Fc fusion proteins by ELISA. Data are pooled from two to three experiments performed in duplicate. **E**. Binding of anti-Mxra8 mAb 9G2.D6 to bacterially-derived mouse Mxra8 and insertion variants Mxra8+5, Mxra8+8, and Mxra8+9, Mxra8+10, Mxra8 +moo, and Mxra8 +[GGS]$_5$ by BLI. Data are the mean and standard deviation of four to eight experiments.
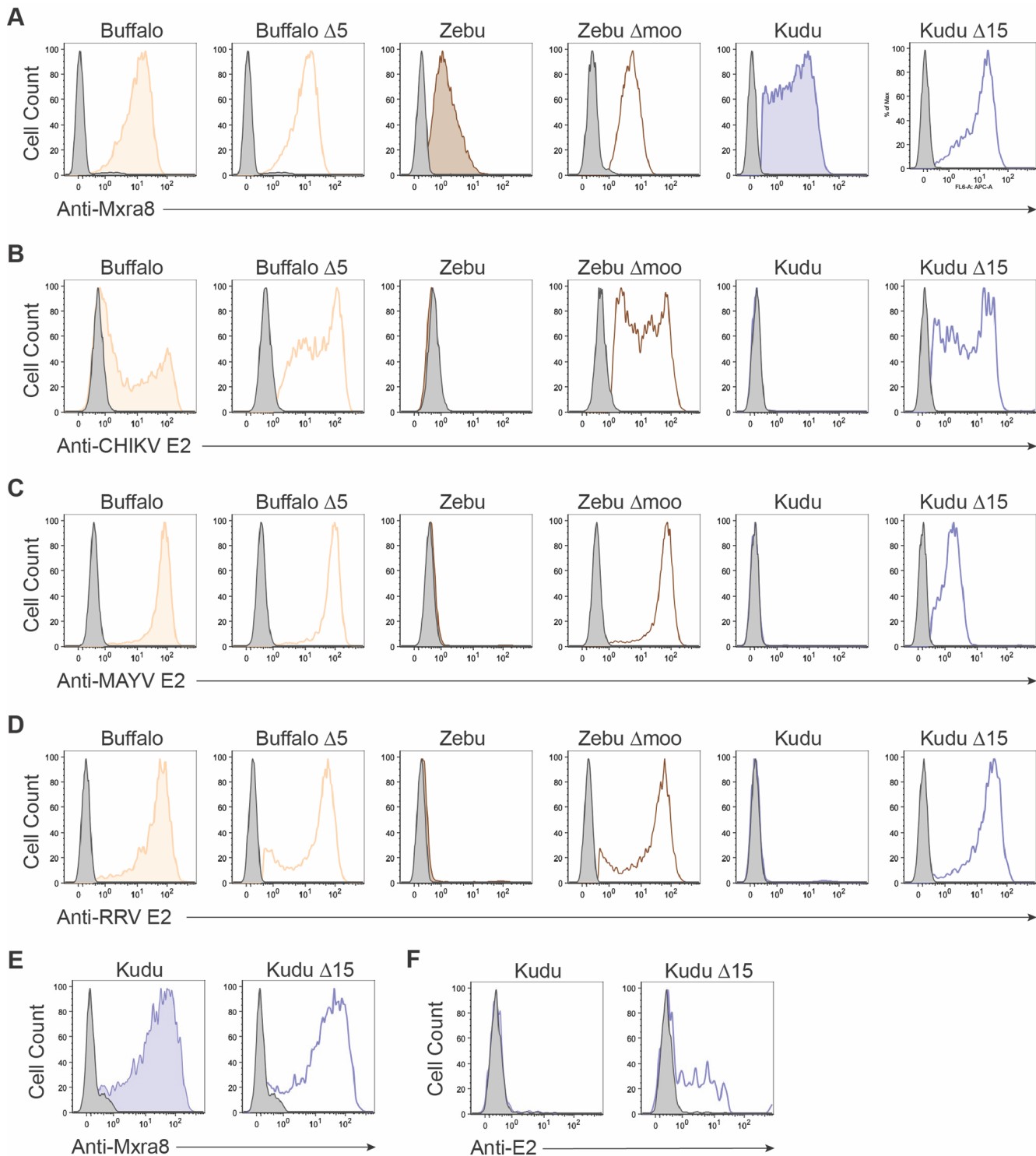
Figure S6. Cell surface expression and alphavirus infection of water buffalo, zebu, and kudu Mxra8 variants, Related to Figure 6. A. Flow cytometry histograms showing cell surface expression of water buffalo, water buffalo Δ5, zebu, zebu Δmoo, kudu, and kudu Δ15 Mxra8 after lentivirus complementation of Δ*Mxra8* 3T3 cells using a pool of anti-Mxra8 mAbs. Data are representative of three experiments. **B-D.** Flow cytometry histograms showing (**B**) CHIKV, (**C**) MAYV, or (**D**) RRV infection of 3T3 Δ*Mxra8* complemented with water buffalo, water buffalo Δ5, zebu, zebu Δmoo, kudu, and kudu Δ15 Mxra8 gene variants. Data are representative of three experiments. **E.** Flow cytometry histograms showing cell surface expression of kudu and kudu Δ15 Mxra8 after lentivirus transduction of primary kudu fibroblasts. Cell surface expression of Mxra8 was detected using a pool of anti-Mxra8 mAbs. Data are representative of two experiments. **F.** Flow cytometry histograms showing MAYV infection of primary kudu fibroblasts complemented with kudu and kudu Δ15 *Mxra8* gene variants. Data are representative of four experiments.
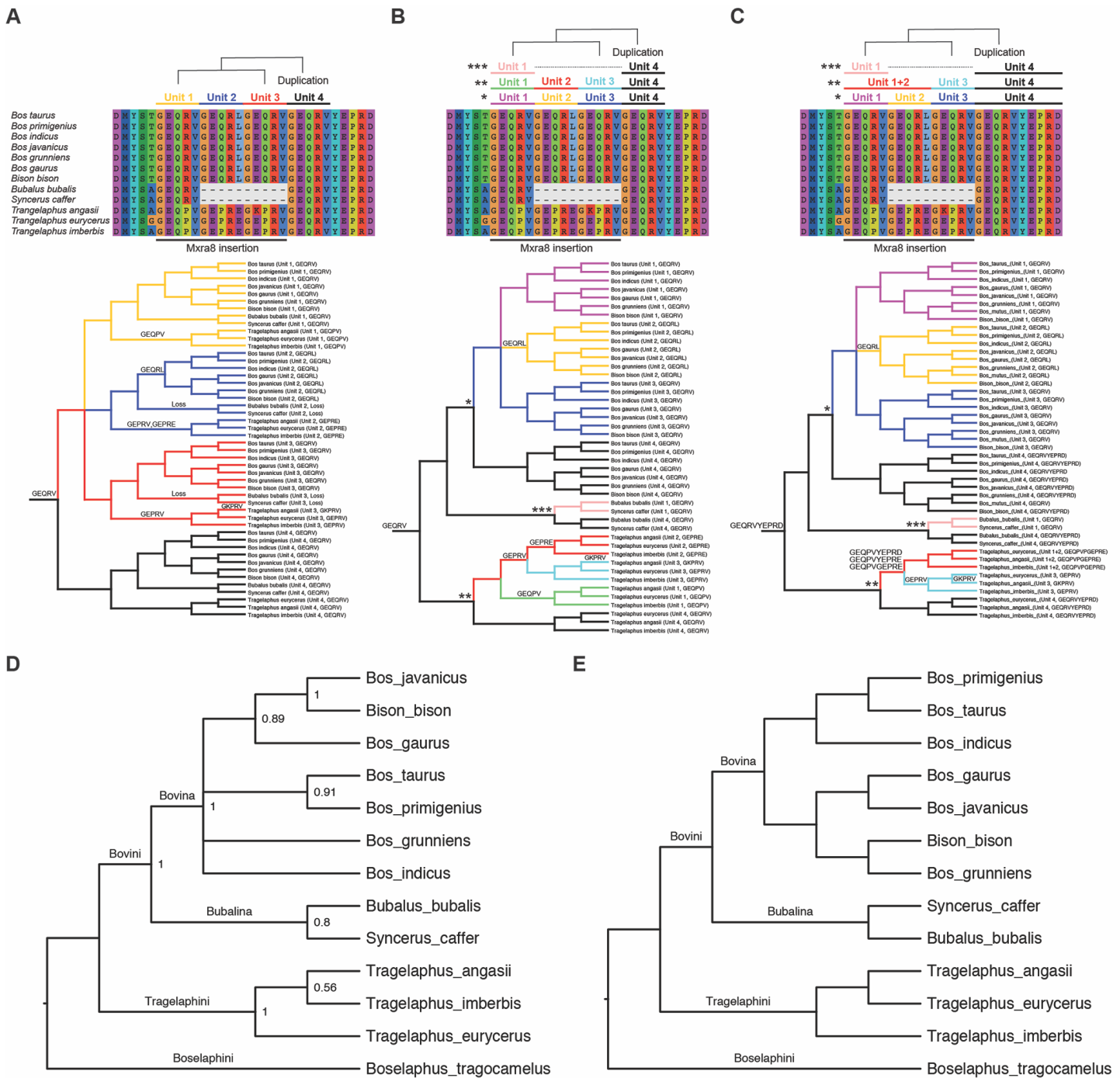
Figure S7. Evolutionary history of Mxra8 insertion, Related to Figure 6. A-C. Three possible evolutionary histories of repeat unit duplication within the Mxra8 insertion, which were reconstructed under maximum parsimony. The sequence alignments (*top panels*) indicate the series of duplications of the insertion repeat units. The Mxra8 insertion is composed of one to three length-5-amino acid sequences (repeat units), where each unit resembles either the length-5 (GEQRV) or potentially the length-10 (GEQRVYEPRD) unit flanking the 3' end of the insertion that is conserved in all sampled Bovidae species. The Mxra8 insertion is likely derived from this conserved unit through a complex sequence of duplication, loss, and substitution events. To our knowledge, we are not aware of any software suited to reconstructing the complex substitution-duplication-loss history of the Mxra8 insertion due to the short length of the repeat unit (GEQRV). Hence, the substitution-duplication-loss history was manually reconstructed under maximum parsimony in Mesquite. The tips of any historical scenario correspond to repeat units that are homologous through duplication events (i.e., paralogous; colors change at bifurcation event) or speciation events (i.e., orthologous; colors constant at bifurcation event). The sequence alignments above each evolutionary history show how the repeat units relate to the Mxra8 insertion alignment. We considered three scenarios to assert the topology for the repeat unit paralogs. Under the L5 scenario (**A**),

where duplication events are rare and loss events are common, 3 duplication, 2 loss, and 6 nonsynonymous substitution events were reconstructed. Under the D5 scenario (**B**), where duplication events are common and loss events are rare, at least 7 duplication, 0 loss, and 5 nonsynonymous substitution events were reconstructed. Under the D10 scenario (**C**), where the Tragelaphini (nyala and bongo) insertion was duplicated from Unit 4, 6 duplication, 0 loss, and 6 nonsynonymous substitution events were reconstructed. All three phylogenetic histories require at least 5 amino acid substitutions, with the majority (>80%) occurring within older lineages. Loss of insertion unit(s) or changes in the insertion sequence are indicated at branch points and branches (**A-C**, *bottom panels*). To reflect three duplication histories, the Mxra8 insertion and insertion + flank alignments were restructured further to correctly assign homology to sites belonging to the paralogous repeat units within the insertion. In the restructured format, each row of the insertion alignment corresponded to one repeat unit from one species. The insertion + flank alignment was processed in the same way, except the flanking regions were concatenated to the left and right of the progenitor GEQRV repeat unit. **D-E**. Topologies for the Mxra8 gene (**D**) and species (**E**) trees are congruent for backbone relationships among Bovina, Bubalina, Tragelaphini, and Boselaphini. Gene tree topology shows clades with posterior support of $P > 0.5$ (node values). The unrooted Mxra8 gene tree topology from the trimmed alignment of the Bovidae gene sequences described in **Table S4** was estimated using RevBayes. Nucleotide evolution was modeled by an HKY substitution process with flat Dirichlet priors assigned to the exchangeability rates and base frequencies. Site-rate variation was modeled by a discrete +Γ4 model with shape and scale parameters following an exponential prior density with rate of 0.1. Relative prior branch lengths followed a flat Dirichlet distribution, which were multiplied by the tree length, L ~ Exponential(10), to model actual branch lengths. The gene was partitioned by codon site position, where the relative clock rate for each partition was modeled by a lognormal prior density with log-mean equal to 1 and log-sd equal to 0.5. The tree was rooted with *Boselaphus tragocamelus* as the outgroup (Zurano et al., 2019). Analysis scripts and the sequence alignment are available at: https://github.com/mlandis/mxra8_bovinae. The estimated gene tree topology was compared to a synthetic species tree topology that we constructed by grafting the phylogenomic relationships among *Bos taurus*, *Bos indicus*, *Bos grunniens*, *Bison bison*, and *Bison bonasus* inferred by others (Wang et al., 2018) into the broader Bovinae species relationships estimated by (Zurano et al., 2019). **Fig S7D** presents a majority rule consensus topology (p > 0.5) for the Mxra8 gene tree, which shows that the backbone relationships among Bos + Bison, Bubalus + Syncerus, and Tragelaphini have high posterior support (p > 0.99) and are congruent with accepted species tree relationships (**Fig S7E**).

Table S1. Amino acid and nucleotide identity and similarity of Mxra8 orthologs, Related to Figure 1.

	Mouse	Rat	Human	Chimp	Dog	Horse	Cattle	Goat	Sheep	Turkey	Duck	Chicken
Mouse		93.9	78.2	77.5	79.8	82.9	76.5	79.6	79.7	58.4	56.3	58.7
Rat	96.6		79.1	78.4	80.7	83.1	76.1	79.4	79.5	58.4	56.5	58.7
Human	84.5	84.5		98.6	82.7	84.2	80.0	82.9	83.3	59.6	57.8	59.6
Chimp	84.0	84.0	99.1		82.0	83.8	79.3	82.3	82.6	59.1	57.1	59.1
Dog	86.3	86.5	88.1	87.6		88.1	83.7	86.3	86.4	60.8	59.9	60.8
Horse	87.2	87.4	89.0	88.5	92.1		85.6	88.7	89.1	60.0	58.7	60.0
Cattle	81.9	81.5	83.4	83.0	88.0	88.4		93.3	93.1	57.9	55.7	57.9
Goat	85.1	84.7	86.3	85.8	90.5	91.6	94.4		98.7	59.7	57.7	59.7
Sheep	85.3	84.9	86.4	86.0	90.7	92.2	94.4	98.9		60.2	58.2	60.2
Turkey	71.5	71.9	71.5	71.2	72.0	72.8	69.7	71.2	71.6		92.7	99.3
Duck	68.9	69.4	69.2	69.0	70.0	70.8	67.5	69.0	69.3	94.3		92.0
Chicken	71.5	71.9	71.5	71.2	72.0	72.8	69.7	71.2	71.6	100.0	94.3	

	Mouse	Rat	Human	Chimp	Dog	Horse	Cattle	Goat	Sheep	Turkey	Duck	Chicken
Mouse	100.0	92.7	77.6	77.3	78.9	80.6	75.1	77.3	77.7	62.2	63.1	62.9
Rat		100.0	77.8	77.6	78.7	80.5	75.1	77.5	77.9	62.1	63.2	62.7
Human			100.0	99.2	84.5	86.0	80.7	82.9	83.2	62.3	64.9	62.6
Chimp				100.0	84.0	85.8	80.5	82.6	83.0	61.9	64.7	62.2
Dog					100.0	87.4	82.4	84.7	85.0	63.7	65.9	64.4
Horse						100.0	84.3	86.6	87.0	63.5	65.9	64.0
Cattle							100.0	92.9	93.4	60.3	62.4	61.2
Goat								100.0	98.7	61.9	63.9	62.5
Sheep									100.0	62.4	64.4	63.0
Turkey										100.0	88.8	97.3
Duck											100.0	89.2
Chicken												100.0

(*Top*) Amino acid sequences were aligned using MUSCLE and amino acid identity (red) and similarity (yellow) were determined using Ident and Sim. (*Bottom*) Nucleotide sequence identity (red) of Mxra8 orthologs was determined using MUSCLE and Ident and Sim.

Table S2. Crystallographic data collection and refinement statistics for cattle Mxra8, Related to Figure 2.

PDB ID code	6ORT
[a]Resolution range	48.47 - 2.30 (2.38 - 2.30)
Space group	P 6(5) 2 2
Unit cell (Å) a, b, c	77.53, 77.53, 242.35
Total number of reflections	1,434,086 (146,561)
Unique reflections	20,172 (1,913)
Multiplicity	71.1 (76.6)
Completeness (%)	100.0 (100.0)
Mean I/σ(I)	49.2 (3.7)
Wilson B-factor	49.9
R_{merge}	0.146 (2.234)
$CC_{1/2}$	1.000 (0.93)
Reflections used in refinement	19,084 (1,842)
Reflections used for R_{free}	1,004 (97)
R_{work}	0.2180 (0.2683)
R_{free}	0.2416 (0.2899)
Number of non-hydrogen atoms	2,364
protein	2,229
solvent	117
Protein residues	277
RMS(bonds) (Å)	0.002
RMS(angles) (°)	0.44
Ramachandran favored (%)	96.73
Ramachandran allowed (%)	3.27
Ramachandran outliers (%)	0.00
Rotamer outliers (%)	0.00
Clashscore	2.29
Average B-factor(Å^2)	51.7
protein	51.7
solvent	49.8

[a]Values in parentheses refer to the highest resolution shell. Data was collected at ALS Beamline 4.2.2 using an RDI CMOS_8M detector. Data processing was carried out in XDS and refinement in Phenix (Adams et al., 2010).

Table S3. Quantitative analysis of mouse and cattle ∆moo Mxra8 binding to CHIKV VLPs by biolayer interferometry, Related to Figure 3.

	k_{on} (M⁻¹s⁻¹)	k_{off} (s⁻¹)	$t_{1/2}$ (s)	$K_{D, kinetic}$ (nM)	$K_{D, equilibrium}$ (nM)
Mouse	$(1.4 \pm 0.6) \times 10^5$	$(8.3 \pm 2.0) \times 10^{-3}$	86.9 ± 17.3	61.5 ± 13.9	66.4 ± 13.3
Cow ∆moo	$(2.8 \pm 0.7) \times 10^5$	$(1.8 \pm 0.3) \times 10^{-2}$	40.2 ± 8.3	64.2 ± 15.5	72.3 ± 19.9

Data are the mean and standard deviations of three independent experiments.

Table S4. Source and *Mxra8* coverage statistics from whole genome and deposited sequences, Related to Figure 5.

Genus	Species	Common Name	Study Accession	Run Accession	Average alignment coverage per base of insert/insert junction	Minimum number of reads aligned at any base of insert/insert junction	Amino acid sequence of insertion
Bos	taurus	Cow	N/A	NM_001075830	N/A[#]	N/A[#]	GEQRVGEQRLGEQRV
Bos	primigenius	Auroch	PRJNA294709	SRR2465682	Modi et al., 2004	Modi et al., 2004	GEQRVGEQRLGEQRV
Bos	indicus	Zebu	PRJNA360096	XM_019976191	N/A[#]	N/A[#]	GEQRVGEQRLGEQRV
Bos	javanicus	Banteng	PRJNA325061	SRR4035276	3.33	3	GEQRVGEQRLGEQRV
Bos	grunniens	Domestic yak	PRJNA359997	SRR5140177	6.93	6	GEQRVGEQRLGEQRV
Bison	bison	Bison	PRJNA257088	SRR1659060	N/A[%]	N/A[%]	GEQRVGEQRLGEQRV
Bubalus	bubalis	Water buffalo	PRJNA207334	AWWX01000000	Contigs*	Contigs*	GEQRV
Syncerus	caffer	African cape buffalo	PRJNA341313	SRR4104498	7.53	7	GEQRV
Tragelaphus	angasii	Nyala	PRJNA388863	SRR5647659	18.8	16	GEQPVGEPREGKPRV
Ovis	orientalis	Mouflon	PRJEB5463	ERR454948	11.4	10	No insertion
Pseudois	nayaur	Himalayan blue sheep	PRJNA361448	SRR5439716	7.85	7	No insertion
Capra	sibirica	Siberian ibex	PRJNA361447	SRR5260693	6	6	No insertion
Moschus	berezovskii	Dwarf musk deer	PRJNA289641	SRR2098995	256.7	248	No insertion
Cervus	elaphus	Red deer	PRJNA324173	SRR4013902	50.5	48	No insertion

N/A indicates that coverage statistics are not available as sequences were obtained from deposited NCBI sequences[#], RNAseq data[%], or sequence contigs*.

Table S5. Primer sequences and annealing temperatures used to amplify *Mxra8* from primary tissue samples, Related to Fig 5.

Genus	Species	Common Name	Nested Primer	Primer sequence	Annealing Temp (°C)
Bos	taurus	Cow	Outer	FOR: GCGCCTCCGGGCCAGGCGGGCGCCATGGAG REV: CAGAGCTGCTGGCCCAGCCAGGAGCCCAGAGTC	65
			Inner	FOR: CGGGCCTGGGTCCTGCTCTGGAGACTTGTG REV: GCAGTACTCCTTCCTGAACTCTTTGTCCAAGTC	60
Bos	javanicus	Banteng	Outer	FOR: GCGCCTCCGGGCCAGGCGGGCGCCATGGAG REV: CAGAGCTGCTGGCCCAGCCAGGAGCCCAGAGTC	65
			Inner	FOR: CGGGCCTGGGTCCTGCTCTGGAGACTTGTG REV: GCAGTACTCCTTCCTGAACTCTTTGTCCAAGTC	60
Bos	gaurus	Gaur	Outer	FOR: GCGCCTCCGGGCCAGGCGGGCGCCATGGAG REV: CAGAGCTGCTGGCCCAGCCAGGAGCCCAGAGTC	65
			Inner	FOR: CGGGCCTGGGTCCTGCTCTGGAGACTTGTG REV: GCAGTACTCCTTCCTGAACTCTTTGTCCAAGTC	60
Bos	grunniens	Domestic yak	Outer	FOR: GCGCCTCCGGGCCAGGCGGGCGCCATGGAG REV: CAGAGCTGCTGGCCCAGCCAGGAGCCCAGAGTC	65
			Inner	FOR: CGGGCCTGGGTCCTGCTCTGGAGACTTGTG REV: GCAGTACTCCTTCCTGAACTCTTTGTCCAAGTC	60
Bison	bison	Bison	Outer	FOR: GCGCCTCCGGGCCAGGCGGGCGCCATGGAG REV: CAGAGCTGCTGGCCCAGCCAGGAGCCCAGAGTC	65
			Inner	FOR: CGGGCCTGGGTCCTGCTCTGGAGACTTGTG REV: GCAGTACTCCTTCCTGAACTCTTTGTCCAAGTC	60
Bubalus	bubalis	Water buffalo	Outer	FOR: GCGCCTCCGGGCCAGGCGGGCGCCATGGAG REV: CAGAGCTGCTGGCCCAGCCAGGAGCCCAGAGTC	65
			Inner	FOR: CGGGCCTGGGTCCTGCTCTGGAGACTTGTG REV: GCAGTACTCCTTCCTGAACTCTTTGTCCAAGTC	60
Syncerus	caffer	African cape buffalo	Outer	FOR: GCGCCTCCGGGCCAGGCGGGCGCCATGGAG REV: CAGAGCTGCTGGCCCAGCCAGGAGCCCAGAGTC	65
			Inner	FOR: CGGGCCTGGGTCCTGCTCTGGAGACTTGTG REV: GCAGTACTCCTTCCTGAACTCTTTGTCCAAGTC	60
Tragelaphus	eurycerus	Bongo	Outer	FOR: CCATCAGGGCCCGCGACCTCCGAC REV: CCCAGCCAGGAGCCCAGAGTCGCC	67
Tragelaphus	angasii	Nyala	Outer	FOR: GCGCCTCCGGGCCAGGCGGGCGCCATGGAG REV: CAGAGCTGCTGGCCCAGCCAGGAGCCCAGAGTC	68
Tragelaphus	imberbis	Lesser kudu	Outer	FOR: GCGCCTCCGGGCCAGGCGGGCGCCATGGAG REV: CAGAGCTGCTGGCCCAGCCAGGAGCCCAGAGTC	68
Boselaphus	tragelaphus	Nilgai	Outer	FOR: CCATCAGGGCCCGCGACCTCCGAC REV: CCCAGCCAGGAGCCCAGAGTCGCC	67
Muntiacus	muntjak	Indian muntjac	Outer	FOR: GCCATGGAGCTGCGGGCCTGGGTCCTGCTC REV: CAGAGCTGCTGGCCCAGCCAGGAGCCTGGAG	65
			Inner	FOR: CTTGTGCTTCTGCAGAGTTCTGCCGTC REV: GCAGTACTCCTTCCTGAACTCTTTGTCCAAG	60
Odocoileus	virginianus	White-tailed deer	Outer	FOR: GCCATGGAGCTGCGGGCCTGGGTCCTGCTC REV: CAGAGCTGCTGGCCCAGCCAGGAGCCTGGAG	68
			Inner	FOR: CTTGTGCTTCTGCAGAGTTCTGCCGTC REV: GCAGTACTCCTTCCTGAACTCTTTGTCCAAG	60

Table S6. Summary of Bovinae Mxra8 insertion evolution, Related to Figure 6.

Evolutionary scenario	Duplication or loss events preferred?	Length of repeat unit	Minimum event counts			
			Duplication	Loss	Nonsynonymous substitution	Synonymous substitution
L5 insert only	Loss	5	3	2	6	1
D5 insert only	Duplication	5	7	0	5	1
D10 insert only	Duplication	5 or 10	6	0	6	2
L5 insert+flank	Loss	5	3	2	8	2
D5 insert+flank	Duplication	5	7	0	7	2
D10 insert+flank	Duplication	5 or 10	6	0	8	3

Evolutionary scenarios and minimum event counts correspond to **Fig S7A-C**. Three proposed evolutionary scenarios explain the distribution of Mxra8 insertions among Bovinae lineages: (1) adaptive inheritance; (2) neutral inheritance; or (3) adaptive introgression. Scenarios are distinguished by the order and geological timing of their evolutionary events and, in particular, whether the events are ancient (millions of years ago) or recent (within the past ten to hundred thousand years). Each evolutionary scenario involves the origin of the Mxra8 insertion one to three times before Bovini, Bubalina, and Tragelaphini originated, followed by an adaptive phase that imprinted detectable patterns of selection within the Mxra8 insertion. The "adaptive introgression" scenario also requires introgression of the insertion between Bovinae species. Under the "adaptive inheritance" scenario, the insertion originates and acquires an adaptive role before Bovinae (or, at latest, before Tragelaphini) first diversifies millions of years ago. The insertion, and any acquired amino acid substitutions, are then inherited vertically during speciation. Vertical transmission would implicate the species tree and Mxra8 gene tree to be largely congruent. Adaptive substitutions would fall primarily along deep branches of the phylogeny, with an imbalance of nonsynonymous or synonymous substitutions, depending on whether positive or purifying selection was in effect, respectively. Severe incongruence between the species tree and Mxra8 gene tree, failure to detect positive or purifying selection within the insertion, or disproportionate numbers of substitutions along terminal branches of the tree would render the "adaptive inheritance" scenario unlikely; these features were not observed in our reconstructions. Similar to the "adaptive inheritance" scenario, the "neutral inheritance" also involves the origin and inheritance of the insertion one to three times in Bovinae. In contrast with the "adaptive inheritance" scenario, the insertion would have faced neutral or nearly neutral selection pressures after it first originated. Like the "adaptive inheritance" scenario, the species tree and gene tree topologies would be largely congruent. If the insertion evolved under neutrality across all Bovinae lineages, both synonymous and nonsynonymous substitutions would be distributed randomly throughout the Bovinae phylogeny. Alternatively, the insertion might have evolved neutrally and only recently faced new selection pressures, in which case nonsynonymous substitutions should be concentrated in the terminal lineages of the phylogeny. However, we reconstructed at least five nonsynonymous and zero synonymous substitutions along internal branches, and only one nonsynonymous and one synonymous substitution along the terminal lineages. Therefore, the sequence data do not appear to support the "neutral inheritance" scenario. Finally, the "adaptive introgression" scenario is designed to allow the insertion to be far younger than the age of Bovinae and assumes that (1) the Mxra8 insertion was deleterious in Bovinae (i.e., insertions would have been rapidly lost) before acquiring a recent adaptive role; (2) as the insertion is found in most extant Bovinae, it must have occurred recently enough to have survived, but too recently to have been inherited vertically while Bovina, Bubalina, and Tragelaphini diversified; and (3) the insertion instead must have been inherited horizontally in the recent past, most likely through numerous introgression events between distantly related Bovinae lineages. If the introgression scenario was true, the Mxra8 gene tree topology should be incongruent with the species tree, and variation in chromosome count in Bovinae should be low. However, the gene tree and species tree estimates are topologically congruent and chromosome counts are highly variable in Bovinae. Thus, the "adaptive introgression" scenario appears unlikely. Of the three evolutionary scenarios considered, our reconstructions are most consistent with the "adaptive inheritance" scenario as described above. If the sequence identity of the Mxra8 insertion has indeed been shaped by selection, it remains to be determined as to what selective force or forces are responsible for those changes

Table S7. Clade ages of Bovinae members, Related to Figure 6.

Clade	Minimum age (Ma)	Maximum age (Ma)	*Mxra8* insertion calibration scenario
Bovinae	14.0	17.6	-
Bovini + Tragelaphini	13.5	16.6	L5
Tragelaphini	6.5	8.1	D5, D10
Bovini	9.4	12.0	-
Bubalus + Syncerus	5.0	8.2	-
Bos	3.4	4.9	-
Bubalus	1.1	2.0	-

Minimum and maximum clade ages are equal to the 95% highest posterior densities estimated by Zurano et al., 2018. Calibration scenarios identify the minimum clade age that corresponds to each of the Mxra8 insertion histories shown in **Fig S7**.

Table S8. Chromosome counts and geographical ranges for selected Mxra8 species, Related to Figure 6.

Family	Subfamily	Tribe	Species name	Chromosome count (2N)	Geographical range
Bovidae	Bovinae	Tragelaphini	*Tragelaphus angasii*	55	South Africa
Bovidae	Bovinae	Tragelaphini	*Tragelaphus imberbis*	38	East Africa
Bovidae	Bovinae	Tragelaphini	*Tragelaphus eurycerus*	34F/33M	African rainforests
Bovidae	Bovinae	Tragelaphini	*Taurotragus oryx*	32F/31M	South and East Africa
Bovidae	Bovinae	Boselaphini	*Boselaphus tragocamelus*	46	South Asia
Bovidae	Bovinae	Bovini	*Bubalus bubalis*	50	South, East and Southeast Asia
Bovidae	Bovinae	Bovini	*Syncerus caffer*	54–56	Sub-Saharan Africa
Bovidae	Bovinae	Bovini	*Bos taurus*	60	Cosmopolitan
Bovidae	Bovinae	Bovini	*Bos javanicus*	60	Southeast Asia
Bovidae	Bovinae	Bovini	*Bos gaurus*	58	South and Southeast Asia
Bovidae	Bovinae	Bovini	*Bos grunniens*	60	Himalayas
Bovidae	Bovinae	Bovini	*Bison bonasus*	60	Europe
Bovidae	Caprinae	Caprini	*Pseudois nayaur*	56	Himalayas
Bovidae	Caprinae	Caprini	*Ovis orientalis*	54	Eurasia
Cervidae	Cervinae	Muntiacini	*Muntiacus muntjak*	6F/7M	Southeast Asia
Cervidae	Cervinae	Cervini	*Cervus elaphus*	68	Northern hemisphere

Chromosome data is sourced from the Atlas of Mammalian Chromosomes (O'Brien, 2006). Geographical ranges based on Global Biodiversity Information Facility records (https://gbif.org) that were filtered for quality.